JOURNAL OF PETROLOGY | VOLUME 37 | NUMBER 6 | PAGES 1547–1577 | 1996

T. C. FEELEY* AND M. A. DUNGAN
DÉPARTEMENT DE MINÉRALOGIE, UNIVERSITÉ DE GENÈVE, 13 RUE DES MARAÎCHERS, 1211 GENÈVE 4, SWITZERLAND

Compositional and Dynamic Controls on Mafic–Silicic Magma Interactions at Continental Arc Volcanoes: Evidence from Cordón El Guadal, Tatara–San Pedro Complex, Chile

Heterogeneous andesitic and dacitic lavas on Cordón El Guadal bear on the general problem of how magmas of differing compositions and physical properties interact in shallow reservoirs beneath continental arc volcanoes. Some of the lavas contain an exceptionally large proportion (<40%) of undercooled basaltic andesitic magma in various states of disaggregation. Undercooled mafic magma occurs in the silicic lavas as large (<40 cm) basaltic andesitic magmatic inclusions, as millimeter-sized crystal-clots of Mg-rich olivine phenocrysts plus adhering Ca-rich plagioclase microphenocrysts (An_{50-70}), and as uniformly distributed, isolated phenocrysts and microphenocrysts. Compositions and textures of plagioclase phenocrysts indicate that inclusion-forming magmas are hybrids formed by mixing basaltic and dacitic melts, whereas textural features and compositions of groundmass phases indicate that the andesitic and dacitic lavas are largely mechanical mixtures of dacitic magma and crystallized basaltic andesitic magma. This latter observation is significant because it indicates that mechanical blending of undercooled mafic magma and partially crystallized silicic magma is a possible mechanism for producing the common porphyritic texture of many calc-alkaline volcanic rocks. The style of mafic–silicic magma interaction at Cordón El Guadal was strongly dependent upon the relative proportions of the endmembers. Equally important in the Guadal system, however, was the manner in which the contrasting magmas were juxtaposed. Textural evidence preserved in the plagioclase phenocrysts indicates that the transition from liquid–liquid to solid–liquid mixing was not continuous, but was partitioned into periods of magma chamber recharge and eruption, respectively. Evidently, during periods of recharge, basaltic magmas rapidly entrained small amounts of dacitic magma along the margins of a turbulent injection fountain. Conversely, during periods of eruption, dacitic magma gradually incorporated small parcels of basaltic andesitic magma. Thus, the coupled physical–chemical transition from mixed inclusions to commingled lavas is presumably not coincidental. More likely, it probably provides a partial record of the dynamic processes occurring in shallow magma chambers beneath continental arc volcanoes.

KEY WORDS: *Chile; commingling; magma mixing; magmatic inclusions*

INTRODUCTION

Geochemical investigations of calc-alkaline lavas and plutons have suggested that mixing of contrasting magmas can account for the compositional features of many comagmatic suites (e.g. Eichelberger, 1975; Anderson, 1976; Langmuir *et al.*, 1978; Koyaguchi, 1986; McMillan & Dungan, 1986; Barnes *et al.*, 1995; Gardner *et al.*, 1995). The physical mechanism responsible for creating such mixtures is commonly linked to forcible injection of mafic magma into subvolcanic silicic magma chambers (Campbell & Turner, 1989; Pallister *et al.*, 1992; Gardner *et al.*, 1995), or turbulent mixing of contrasting magmas during eruption of zoned chambers (Koyaguchi, 1985; Blake & Ivey, 1986; Cioni *et al.*, 1995). In addition, in a few examples, mixing both before and during eruption may have occurred (Freundt &

*Corresponding author. Present address: Department of Earth Sciences, Montana State University, Bozeman, MT 59717, USA

Schmincke, 1992; Blake *et al.*, 1992). Although providing a satisfactory explanation for geochemical relations, simple liquid–liquid blending is unlikely to have occurred in systems where the endmembers differ greatly in temperature and viscosity, and where there is a small proportion of the mafic endmember, typically 50% or less (Sparks & Marshall, 1986; Frost & Mahood, 1987). Below this limit the mafic magma is prevented from mixing with the volumetrically dominant silicic magma owing to formation of isolated undercooled inclusions (e.g. Bacon, 1986). Consequently, it has been suggested that mechanical disaggregation and dispersion of these inclusions may be a physically more realistic process for creating geochemical trends that mimic those of magma mixing (Bacon & Metz, 1984; Thompson & Dungan, 1985; Koyaguchi, 1986; Clynne, 1996).

In this paper the efficacy of magma mixing is addressed in the context of our petrologic study of andesitic and dacitic lavas present at Cordón El Guadal in the Tatara–San Pedro complex, Andean Southern Volcanic Zone. Lavas present at Cordón El Guadal are unique in the Tatara–San Pedro complex because many contain an exceptionally large volume (20–40%) of undercooled inclusions of basaltic andesitic magma. Earlier work presented bulk-rock geochemical trends in support of mixing between basaltic andesitic magma and, in some cases, unrealistically large amounts of dacitic magma (0–100%) within the Guadal magmatic system (Davidson *et al.*, 1988).

Our objectives here are to describe in detail the compositions and textures of phenocrysts and groundmass minerals present in coexisting inclusion–host lava pairs, and to use these data to: (1) infer whether the minerals are in equilibrium with their respective bulk-rock and groundmass liquids, (2) calculate the temperatures and H_2O contents of the subvolcanic magma chambers, and finally, (3) construct a physical model for the evolution of shallow crustal magma chambers in the Guadal system so as to better understand the complex mechanisms by which mafic and silicic magmas interact at continental arc volcanoes. The mineral compositions and textures of Guadal lavas are best explained by the following process: (1) mixing of dacitic magma into inclusion-forming magma while both were partially molten, followed by (2) post-undercooling mechanical disaggregation of largely crystallized magmatic inclusions and dispersion into host dacitic magma (commingling). We infer that the mixing and commingling were separate events associated with periods of recharge and eruption of stratified magma chambers, respectively.

GEOLOGIC OVERVIEW

Tatara–San Pedro complex: local geology

The Tatara–San Pedro complex is a frontal arc stratovolcanic complex located in the northern half of the Andean Southern Volcanic Zone at 36°S, 70·5°W. The complex consists of mid-Pleistocene (0·930 Ma) to Holocene lavas, volcaniclastic rocks, pyroclastic units, and shallow intrusive rocks (Singer *et al.*, 1996). Geologic and stratigraphic relations record at least eight major periods of edifice construction with intervening erosional hiatuses.

The most prominent edifices of the complex are two large stratovolcanoes (Fig. 1). Volcán Tatara–San Pedro proper, the highest (3621 m) and youngest of the two, is a composite cone consisting of a large (22 km^3) late Quaternary (90–19 ka) basaltic andesitic to andesitic construct (Volcán Tatara), which is mantled by volumetrically minor ($<0·5$ km^3) basaltic andesitic to dacitic lavas erupted from Holocene vents (Volcán San Pedro; Ferguson *et al.*, 1992). The older stratovolcano, Volcán Pellado (240–176 ka), is located ~5 km northeast of Tatara–San Pedro. It is deeply dissected by glacial erosion to the extent that much of the central vent region is no longer preserved. Evidence for its previous existence, however, is provided by steeply dipping, locally hydrothermally altered andesitic lavas and pyroclastic units, and a volcanic plug. In addition to the two main stratovolcanoes, the deeply eroded remains of a basaltic to rhyolitic center are located at the head of Cajón Huemul in the northern region of the complex (not shown in Fig. 1). The original volume of this center is impossible to estimate because it has been largely removed by glacial erosion. The vent location, however, is well delimited to within a region containing strong hydrothermal alteration and a concentration of northeast-striking faults and andesitic to rhyolitic dikes.

Preserved volcanic rocks at the complex are mainly (~80%) basaltic to basaltic andesitic (50–57% SiO_2) lavas. Exceptions to these dominantly mafic compositions include andesitic to dacitic lavas (58–69% SiO_2) that erupted throughout the entire history of the complex, and eruption of a single large rhyolitic lava flow during the early stages of extrusive activity at 853 ± 15 ka (Singer *et al.*, 1996). These temporal variations in bulk chemistry appear to reflect continuous injection of mafic magma into the shallow crust beneath the complex, and episodic production of small volumes of silicic magma by either differentiation or crustal melting, or both.

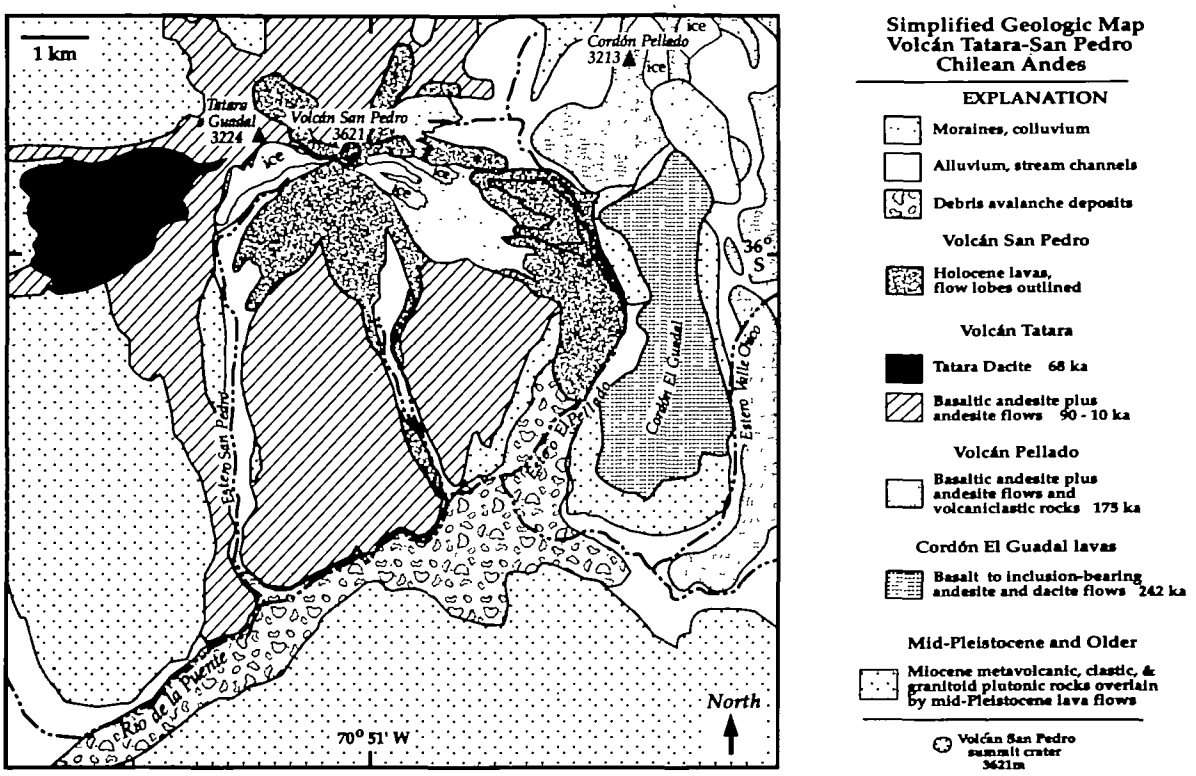

Fig. 1. Simplified geologic map of Volcán Tatara–San Pedro and Cordón El Guadal.

Cordón El Guadal lavas

The sequence of lavas which is exposed on Cordón El Guadal (<600 m thick), and on the lower slopes of the distal west wall of Estero Pellado, range from thick dacitic lavas (>100 m) to much thinner basaltic and basaltic andesitic lavas (<10 m). Because the pre-Guadal topographic relief was in excess of 200 m, thickness is also locally controlled by ponding of large early lavas. A few thin pyroclastic units are interbedded with lavas on the north end of Cordón El Guadal, and one small erosional remnant of a densely welded andesitic ash-flow tuff is preserved on the crest. Thinning of the lavas and primary dips to the SSE indicate a buried or eroded source to the NNW of Cordón El Guadal.

A notable feature of the Guadal sequence is that all of the andesitic and dacitic lavas contain undercooled inclusions of basaltic andesitic magma (hereafter referred to as magmatic inclusions). In dacitic and higher-silica andesitic lavas these magmatic inclusions are large (<40 cm across) and abundant (20–40%), whereas in lower-silica andesitic lavas they are rare (<5%) and small (<10 cm). In some thick dacitic flows the inclusions are strongly concentrated at the top of the flow (particularly the units represented by samples Gua3 and Gua20 plus Gua21). By analogy with zoned ash-flow tuffs, we suggest that such a distribution may reflect concentration of basaltic andesitic magmas beneath silicic magmas in the pre-eruptive magma chambers. However, in others (e.g. Gua12), the inclusions occur distributed more or less homogeneously throughout the lava. Many inclusions appear to be small, texturally homogeneous broken or abraded fragments from originally larger inclusions. These lack the globular, pillow-like morphologies and fine-grained rims that characterize many chilled inclusions (see Bacon, 1986).

The Guadal sequence does not define a progressive differentiation sequence. Rather, the entire range in composition appears to be randomly distributed throughout the section. Dacitic lavas occur both near the base (Gua3) and near the top of the sequence (Gua12), as do mafic lavas (Gua2 vs Gua13 plus Gua14, respectively). Thus, each magma composition in this volcanic suite must be considered a unique end-product of multiple differentiation processes, rather than a direct predecessor to another magma composition.

METHODS

Modal compositions of Guadal samples were determined by calculating the average percent area occupied by individual mineral species over six ~30 mm^2 areas, using the image analysis software Optimas®. Silicate mineral phases were manually distinguished and their areas delimited in transmitted light. Oxide phases were identified and delimited automatically by the software in reflected light. Phenocrysts are defined as >0·5 mm, except oxide phenocrysts, which are >0·25 mm.

Mineral compositions and analyses of glassy and cryptocrystalline groundmass were determined at the University of Lausanne, Switzerland, on a Cameca SX50 electron microprobe using ZAF on-line data reduction and matrix correction procedures. A 15 kV accelerating voltage was used with a 10 nA specimen beam current for plagioclase and groundmass and 20 nA for all other minerals. To minimize Na loss during analyses of the groundmass, we used a continuously rastering, defocused beam (~10 μm), following the technique of Luhr (1992). Compositionally dependent textural features of plagioclase were investigated using Nomarski differential interference contrast microscopy (Anderson, 1983). Major and trace element concentrations were determined by X-ray fluorescence (XRF) following the techniques described by Rhodes (1988).

CHEMICAL COMPOSITIONS

Representative chemical and modal analyses of Guadal volcanic rocks are presented in Table 1. Table 2 contains groundmass analyses for seven andesitic and dacitic lavas. Compositions of the volcanic rocks are calc-alkaline and they range from medium-K basaltic to high-K dacitic (Fig. 2). There are small gaps in the SiO_2 contents of the lavas from 53·9 to 56·7 wt % and from 63·6 to 64·9 wt %. These gaps are probably not artifacts of incomplete sampling or analytical error because the data illustrated in Fig. 2 represent every lava flow present on Cordón El Guadal and they exceed the analytical uncertainty of the analyses (~ ±0·5% SiO_2; Rhodes, 1988). Instead, as discussed in more detail below, they have genetic significance because the gap at lower SiO_2 contents is filled by compositions of the magmatic inclusions, and the gap at higher SiO_2 contents is associated with subtle inflections in the trends for a few elements (e.g. Na_2O, K_2O, MgO).

Concentrations of compatible major and trace elements (e.g. MgO, Ni, Cr) in basaltic and basaltic andesitic lavas and a few magmatic inclusions (e.g. Gua6.MI) are low and decrease rapidly with increasing SiO_2, suggesting fractionation of ferromagnesian silicate and oxide phases (solid Fx trend, Fig. 2). In addition, in the mafic lavas concentrations of CaO are constant, and Al_2O_3 and Na_2O increase with increasing SiO_2. In accord with petrographic features (see below), these relations suggest that the mafic lavas have also accumulated plagioclase. Similar increases in Al_2O_3 and Na_2O are not observed for the fractionated inclusions.

In contrast to the mafic lavas, the basaltic andesitic inclusions and the andesitic and dacitic lavas have elevated concentrations of both compatible and incompatible elements. Data for the inclusions and andesitic lavas define arrays that are linear and continuous from ~55% to ~64% SiO_2. Trends for the dacitic lavas are separated from these arrays by the above-mentioned gap of 1·3 wt % SiO_2. Groundmass glasses of the andesitic and dacitic lavas are high-K rhyolitic and they are characterized by lower MgO, FeO, Al_2O_3, Na_2O, and higher K_2O than the dacitic lavas. Although the low Na_2O contents of some groundmass glasses suggest the possibility of alkali loss during the microprobe analyses, correlated decreases in Na_2O, CaO, and Al_2O_3 with increases in K_2O and SiO_2 are better accounted for by crystallization of plagioclase from high-K dacitic and rhyolitic liquids.

With respect to identification of potential differentiation processes affecting the Guadal suite, the two most important features of the whole-rock chemical analyses are the steeply decreasing compatible element trends in the mafic lavas and the lower slopes of the linear arrays defined by the magmatic inclusions and andesitic lavas. The latter feature is of particular interest because continuous linear major and trace element trends are considered general characteristics of igneous rock suites related by simple two-component magma mixing (e.g. Langmuir *et al.*, 1978; McMillan & Dungan, 1986). For example, Davidson *et al.* (1988) also noted these linear trends and suggested that the Guadal andesitic lavas represent blended hybrids. In detail, however, the linear trends for the Guadal suite appear to violate physical constraints on the mixing of two compositionally distinct liquids because the large array of lava compositions implies proportions of the basaltic andesitic endmember from 100 to 0% (Fig. 2). As discussed by Thompson & Dungan (1985), complete mixing of such compositionally disparate liquids to form a single homogeneous magma is inhibited by rapid crystallization of the hot mafic endmember upon incorporation into cooler silicic melt. Sparks & Marshall (1986) and Frost & Mahood (1987) have suggested that true liquid mixing is realistic only for systems that contain >50% of a mafic endmember. The smaller

Table 1: Representative major, trace, and modal analyses of volcanic rocks from Cordón El Guadal

Sample:[1]	14	6.MI	3B.MI	21.MI	13	9	6	24	21	3	12
SiO_2	51·30	54·42	55·20	56·61	57·39	60·74	61·44	63·25	65·75	66·63	67·46
TiO_2	1·07	1·05	0·79	0·75	0·85	0·72	0·83	0·68	0·63	0·62	0·52
Al_2O_3	17·58	18·40	18·22	17·69	17·05	16·73	16·69	16·14	15·88	16·02	15·57
FeO*	8·90	7·75	7·01	6·44	6·24	5·35	5·42	4·73	3·94	3·78	3·26
MnO	0·16	0·13	0·13	0·12	0·11	0·11	0·11	0·10	0·09	0·08	0·08
MgO	6·74	3·99	5·36	4·70	4·79	3·49	2·51	2·75	1·45	1·29	1·37
CaO	8·64	8·33	7·38	6·90	7·01	5·33	5·07	4·51	3·36	3·21	3·01
Na_2O	3·59	3·63	3·57	3·83	3·79	4·23	4·29	4·43	4·66	4·78	4·69
K_2O	0·86	1·17	1·37	1·63	1·84	2·42	2·59	2·71	3·26	3·27	3·41
P_2O_5	0·22	0·23	0·16	0·16	0·24	0·16	0·21	0·16	0·16	0·15	0·13
Total	99·04	99·10	99·19	98·83	99·32	99·28	99·16	99·46	99·16	99·82	99·49
Zr	89	117	96	118	146	189	223	208	246	248	237
Sr	550	530	635	577	686	470	388	376	308	301	292
Ni	59	11	58	57	55	36	13	22	11	11	6
Cr	93	54	103	97	99	56	11	44	4	2	0
V	193	162	146	139	143	102	112	86	52	58	56
Ba	279	347	373	374	422	449	484	514	563	583	577
Y	17	17	15	15	15	17	21	19	20	20	17
Sr	542	528	628	577	675	468	387	382	314	303	291
U	1	0	1	1	2	3	4	4	5	4	5
Rb	16	31	30	44	53	77	87	90	112	109	116
Th	2	3	5	6	7	10	10	11	14	13	16
plag	20·0	6·3	4·3	9·4	2·6	7·8	17·3	11·3	21·2	18·3	7·2
ol	6·6	0·5	3·6	1·0	2·1	0·8	0·2	0·5	0·2	0·2	0·1
cpx	—	0·1	0·6	0·6	2·6	0·3	2·6	3·0	1·2	1·8	0·2
opx	—	tr.	tr.	tr.	tr.	0·4	1·5	tr.	0·5	0·5	0·3
oxide	tr.	0·3	0·1	0·4	0·0	0·6	0·5	0·5	0·8	0·5	0·4
total pheno.	26·6	7·1	8·5	11·4	7·4	9·8	22·1	15·3	24·0	21·3	8·2

[1]Samples with MI suffix are magmatic inclusions.
*In this and most succeeding tables, total Fe reported as FeO.

proportions of mafic components in many Guadal lavas thus appear to require an alternative process that mimics the elemental expression of two-component mixing. Bearing this physical constraint in mind, we discuss in the following section petrographic features of the Guadal eruptive products with the aim of better understanding the processes responsible for the development of compositional diversity in this system.

PETROGRAPHY

Basaltic and basaltic andesitic lavas

Variations in modal phenocryst abundances with respect to bulk SiO_2 content are illustrated in Fig. 3. Guadal basaltic and basaltic andesitic lavas contain 18–28% by volume phenocrysts of plagioclase, olivine (with Cr-spinel inclusions), and rare clinopyroxene. Plagioclase is by far the most abundant phase, accounting for 75–90% of the assemblage in all samples (Table 1). Some of these grains are coarsely embayed or finely sieved. The latter texture is defined by a diffuse network of isolated glass inclusions that are usually concentrated in a narrow band inward a few tens of microns from the crystal margin (Fig. 4a). There appears to be no compositional distinction between clear, embayed, or sieved grains, however. Textures with increasing SiO_2

Table 2: Groundmass analyses, plagioclase rims, and estimated melt H_2O contents

Sample:	Gua13	Gua9	Gua6	Gua11	Gua21	Gua3A	Gua12
Groundmass							
SiO_2	74·87	73·00	71·32	72·47	73·97	73·32	73·02
Al_2O_3	12·56	13·74	15·22	15·46	13·00	13·51	13·98
FeO*	0·79	1·23	1·76	1·56	1·37	1·44	1·00
MgO	0·03	0·11	0·42	0·36	0·12	0·28	0·42
CaO	1·26	0·98	1·37	1·23	1·11	1·42	1·62
Na_2O	3·61	4·02	4·45	4·51	4·00	4·52	4·52
K_2O	4·92	5·71	4·57	3·78	5·27	4·17	4·41
Total	98·04	98·79	99·11	99·38	98·83	98·66	98·97
ca-no.[1]	0·16	0·12	0·15	0·13	0·13	0·15	0·17
Plagioclase rims[2]							
SiO_2	58·82	59·87	59·57	59·40	59·58	60·61	56·59
Al_2O_3	25·23	24·52	25·91	25·19	25·04	23·85	26·44
FeO*	0·27	0·38	0·39	0·37	0·33	0·37	0·50
MgO	0·02	0·02	0·02	0·01	0·02	0·01	0·04
CaO	7·38	6·70	6·90	6·91	6·73	7·06	9·16
Na_2O	6·93	7·25	7·09	7·18	7·36	7·25	6·19
K_2O	0·73	0·83	0·84	0·81	0·53	0·84	0·52
Total	99·38	99·57	100·71	99·87	99·59	99·98	99·44
An %	35·5	32·2	33·3	33·1	32·6	33·4	43·6
T (°C)[3]	955	945	956	890	902	883	922
H_2O (Ab)	1·5	1·7	2·0	3·3	2·2	3·1	2·8
H_2O (An)	1·3	1·8	2·7	3·8	2·2	3·0	2·2
Ab–An	0·2	–0·1	–0·7	–0·5	0·0	0·1	0·6

[1] *ca*-no. is Ca/(Ca + Na).
[2] Rim compositions are averages of Type 1 and 2 phenocrysts in lavas.
[3] Temperature estimates are average of estimates from Fe–Ti oxide (Table 5) and pyroxene (Table 4) thermometry. Melt water contents calculated using the albite (Ab) and anorthite (An) exchange reactions described by Housh & Luhr (1991). Analytical techniques discussed in text.

range from seriate to strongly porphyritic. The nearly holocrystalline groundmasses consist of trachytically aligned plagioclase, clinopyroxene, and Fe–Ti oxides.

Andesitic and dacitic lavas

Guadal andesitic and dacitic lavas have a wide range in both modal proportions of total phenocrysts and individual mineral species, although the mineral assemblage varies little throughout the compositional spectrum (Table 1; Fig. 3). The lavas contain 8–27% euhedral to subhedral phenocrysts with the total increasing linearly with increasing bulk-rock SiO_2 contents (excluding the highest SiO_2 lava). This increase in total phenocrysts is mirrored by linearly increasing amounts of plagioclase, which accounts for ~75% of the mineral assemblage of most andesitic and dacitic lavas, except for those with the lowest SiO_2 contents, in which modal proportions decrease to ~40%. Proportions of olivine decrease and Fe–Ti oxides increase with increasing SiO_2. Samples with SiO_2 >58 wt% also contain both clinopyroxene and orthopyroxene, whereas orthopyroxene is rare in lower-silica andesitic lavas. Minor amphibole (<0·1%) has been found in only three dacitic lavas. Accessory apatite and, less commonly, zircon occur as microphenocrysts and as inclusions or grains attached to other minerals, particularly oxides. Cr-spinel inclusions are present in many olivine crystals. The groundmass mineral assemblage is similar to the phenocryst assemblage

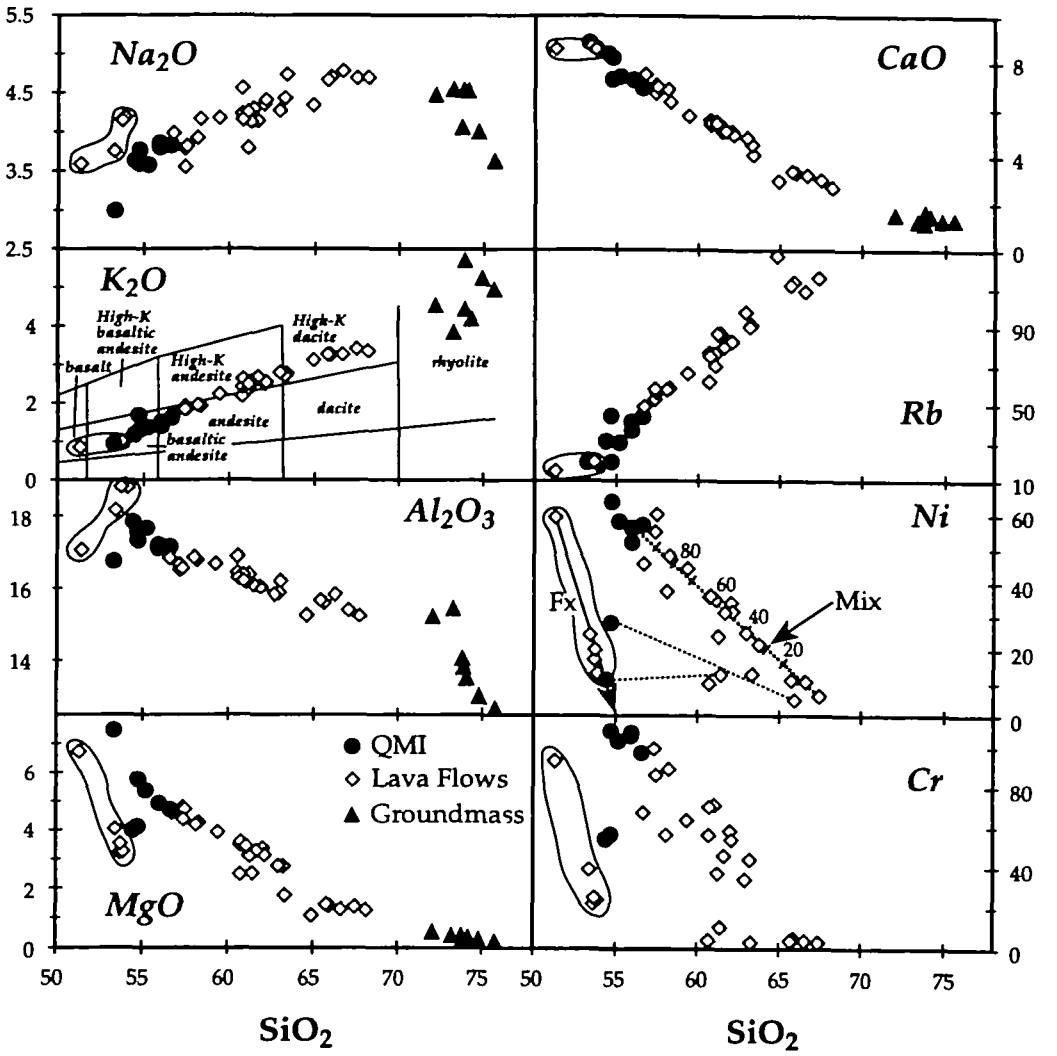

Fig. 2. Variation of select major and trace elements vs wt % SiO_2 for Guadal lavas, magmatic inclusions, and glassy to cryptocrystalline groundmasses of the lavas. The K_2O vs SiO_2 diagram indicates the nomenclature used in this study (Peccerillo & Taylor, 1976). Circled field indicates the range of basaltic and basaltic andesitic lava compositions. The effects of olivine fractionation (continuous Fx curve) and mixing (thick dotted Mix line) are illustrated schematically. Thin dotted tie lines connect fractionated inclusions with coexisting host lavas. Tick marks on the main mixing trend give the proportion of mafic endmember.

except that olivine is absent and the ratio of clinopyroxene to orthopyroxene is higher in the groundmass.

Textural features of the andesitic and dacitic lavas correlate roughly with bulk-rock SiO_2 contents. In general, groundmass microphenocrysts become much less abundant and phenocrysts, although becoming more abundant, show a restricted variation in grain size in lavas with increasing SiO_2 contents. Lower-silica andesitic lavas are characterized by seriate textures because mineral phases (especially plagioclase) range continuously from equant phenocrysts (<3 mm across) to elongated groundmass microphenocrysts (Fig. 4b). Groundmass textures in these samples range from intergranular to intersertal depending upon the degree of groundmass crystallinity (which is usually high). Andesitic lavas have classic porphyritic textures wherein large phenocrysts (<3 mm) are surrounded by a fine-grained groundmass consisting of microlitic plagioclase, pyroxenes, oxides, and abundant interstitial glass (Fig. 4c). Dacitic lavas are hypocrystalline because groundmass phases are sparse. Phenocryst relations are similar to those in the andesitic lavas (Fig. 4d).

In addition to the main textural types described above, nearly all of the andesitic and dacitic lavas are glomeroporphyritic because they contain up to ~10% (typically 1–5%) coarse-grained polycrystalline aggregates, or crystal-clots (see Nakada *et al.*, 1994; Tomiya & Takahashi, 1995). The aggre-

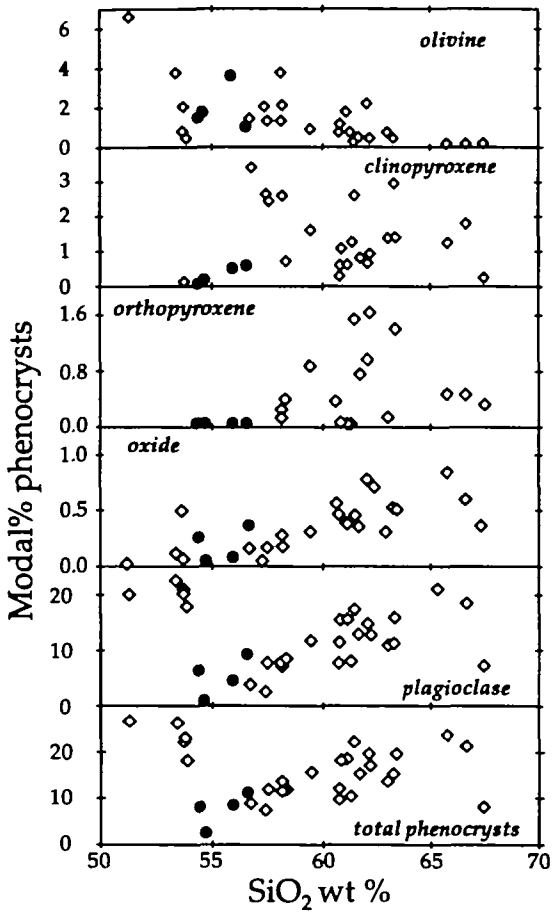

Fig. 3. Variation of modal abundances of phenocryst phases in lavas and magmatic inclusions vs wt % SiO_2. Symbols as in Fig. 2.

gates are usually from 2 to 4 mm across (the largest is 7·5 mm) and are of two textural and mineralogical types. The most common type consists of euhedral plagioclase and oxides complexly intergrown with euhedral to subhedral clinopyroxene, orthopyroxene, or both (Fig. 4d). Olivine has only been observed as an aggregate-forming mineral in the lowest silica andesitic lavas, where it is intergrown with clinopyroxene + plagioclase + oxides. Cores of plagioclase crystals in aggregates lacking olivine are often extremely calcic relative to the average composition of isolated plagioclase phenocrysts (see below).

The other type of aggregate consists of one or a few large olivine, clinopyroxene, or olivine + clinopyroxene grains (+ oxides) and adhering plagioclase microphenocrysts (Fig. 4c). This type of crystal-clot is most abundant in lower-silica andesitic lavas, although they have been observed in all andesitic and dacitic lavas. They are petrographically distinct from the glomerocrysts described above because plagioclase occurs as small, acicular crystals, which contrast with the large, more equant crystals present in those described above, and olivine is common and occurs as fragmented grains or segments detached from larger crystals. These aggregates are derived from mechanical disaggregation of magmatic inclusions contained within the andesitic and dacitic lavas [see below and Clynne (1996)].

Magmatic inclusions

Most of the basaltic andesitic magmatic inclusions contained within the andesitic and dacitic lavas are porphyritic with <1 to 10% total phenocrysts of euhedral to subhedral plagioclase, Fe–Ti oxides, olivine, clinopyroxene, and rare orthopyroxene (Fig. 3). With the exception of low pyroxene abundances, inclusions have individual and total phenocryst contents similar to the lower-silica andesitic lavas, and they fall at the end of the trends formed by all of the dacitic and andesitic lavas in Fig. 3. Groundmass textures are intergranular because they are characterized by numerous acicular to skeletal plagioclase laths in random or subradial arrangement (Fig. 4e). Amphibole occurs as a groundmass phase in the inclusions of one dacitic lava flow (Gua20). Groundmass laths in most inclusions are 0·1–0·4 mm across, although some inclusions contain a few acicular grains that are as coarse as 1·2 mm in the longest dimension. There appears to be no correlation between inclusion composition, host-rock composition, and groundmass lath size or texture, and some lavas contain both coarse- and fine-grained inclusions. Interstices between the plagioclase laths are filled by elongated to equant (but subhedral) microphenocrysts of clinopyroxene and less abundant orthopyroxene, and euhedral Fe–Ti oxides. Glass, although present, is not abundant (usually <10%). All inclusions also contain vesicles and groundmass voids, although most are relatively dense because vesicles are small (<1·0 mm) and not particularly abundant (<10%).

The basaltic andesitic inclusions undoubtedly formed by chilling of hot mafic magma in cooler, more silicic host magma because they have many of the textural criteria described by Bacon & Metz (1984) and Bacon (1986) for recognizing undercooled blobs of mafic magma in volcanic rocks. Specific evidence for undercooling of Guadal inclusions includes: (1) the habits of the groundmass microphenocrysts, which are indicative of crystallization in an undercooled state (see Lofgren, 1974; Corrigan, 1982), (2) vesiculated textures, (3) ellipsoidal shape, and (4) margins that are cuspate and chilled on a few large inclusions.

Textures of many inclusions also suggest the additional process of mechanical disaggregation of inclu-

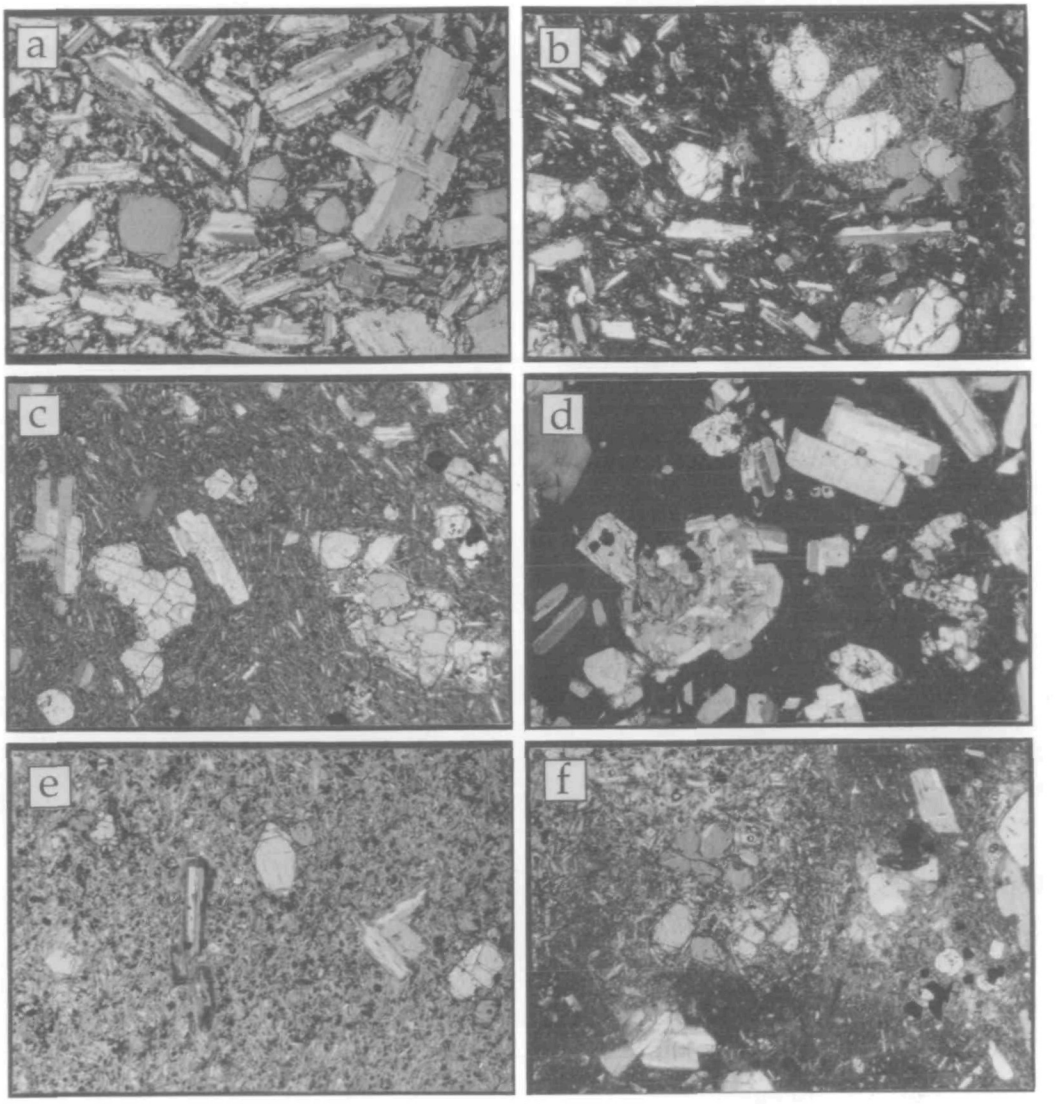

Fig. 4. Photomicrographs showing characteristic textures of Cordón El Guadal lavas and inclusions. All are ~5 mm across with partially crossed polars. (a) Seriate textured basaltic lava (Gua14) with phenocrysts of plagioclase and olivine in holocrystalline groundmass of plagioclase, Fe–Ti oxides, and clinopyroxene. (Note fine sieved band on plagioclase in upper left.) (b) Seriate textured lower-silica andesitic lava (Gua13) with plagioclase, olivine, and clinopyroxene phenocrysts. (Note small olivine-bearing magmatic inclusion in upper right.) (c) Porphyritic textured andesitic lava (Gua9) with Type 1 (center) and 3 plagioclase (left), olivine, and clinopyroxene phenocrysts in a glassy groundmass with plagioclase, clinopyroxene, and Fe–Ti oxide microphenocrysts. (See text for discussion of plagioclase types. Note adhering plagioclase microlites on olivine cluster on right.) (d) Glomeroporphyritic, hypocrystalline dacitic lava (Gua21) with Type 1 plagioclase, clinopyroxene, and orthopyroxene phenocrysts set in glassy groundmass with rare plagioclase and clinopyroxene microphenocrysts. Phenocrysts in glomerocryst (center) are blocky Type 2 plagioclase, clinopyroxene, and Fe–Ti oxides. (e) Porphyritic textured basaltic andesitic magmatic inclusion (Gua3A.MI) with Type 3 plagioclase and olivine phenocrysts set in a fine-grained intergranular groundmass of acicular plagioclase, clinopyroxene, and Fe–Ti oxide phenocrysts plus minor glass. (f) Detail of magmatic inclusion disaggregation in andesitic lava (Gua11). (Note fragmentation of large olivine crystal and dispersal of quench microphenocrysts.)

sions following undercooling. Direct evidence for this process consists of all stages of inclusion disaggregation at both outcrop and thin-section scales. For example, undercooled mafic magma exists in the andesitic and dacitic lavas as inclusions of undercooled basaltic andesitic magma (<40 cm), as the millimeter-sized crystal-clots of Mg-rich olivine phenocrysts plus adhering Ca-rich plagioclase microphenocrysts described above, and as isolated phenocrysts and microphenocrysts uniformly distributed throughout the silicic lavas. Phenocryst- and microphenocryst-laden plumes are observed trailing off inclusions in many thin sections and in outcrop (Fig. 4f). Many lavas also contain both

coarse- and fine-grained small inclusions that show no concentric zonation in vesicle or groundmass crystal size, and which possess margins that are neither cuspate nor quenched. These latter features are identical to the textural features of inclusions described by de Silva (1989), who interpreted his samples as detached pieces of the early crystallized boundary layers of silicic magma chambers. In contrast, we explain them as formed during mechanical abrasion and dispersion of undercooled basaltic andesite magma, such that the small coarse-grained inclusions represent the relatively slowly cooled interior regions of larger inclusions, and the fine-grained inclusions represent more rapidly cooled regions closer to the originally chilled, but now eroded margins (Linneman & Myers, 1990; Nakada *et al.*, 1994).

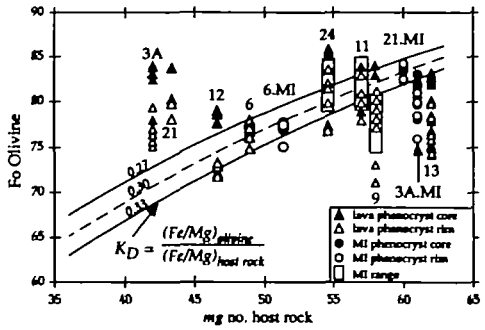

Fig. 5. Forsterite (Fo) contents of olivine phenocryst cores and rims vs molar *mg*-numbers [100Mg/(Mg + Fe^{2+})] of Guadal lavas and magmatic inclusions. Each point represents an analysis. Shaded fields behind lava samples Gua24, Gua11, and Gua9 indicate ranges of olivine analyses in coexisting magmatic inclusions for which no whole-rock analyses exist. Lines represent equilibrium between minerals and whole-rock compositions. The lines were calculated assuming: (1) NNO buffer equation of Heubner & Sato (1970); (2) whole-rock *mg*-number calculated by the equation of Kilinc *et al.* (1983); (3) 1100°C for basaltic andesites, 950°C for andesites, and 900°C for dacites; and (4) equilibrium $^{Fe/Mg}K_{D\ min/liq}$ values of 0·27–0·33 (Roeder & Emslie, 1970).

MINERALOGY AND MINERAL–MELT EQUILIBRIA

Olivine

Olivine occurs in andesitic and dacitic lavas as isolated, euhedral to subhedral phenocrysts up to 2 mm across, and in crystal clots with adhering plagioclase microphenocrysts. In these lavas olivine phenocrysts are always fractured, and many subhedral crystals are fragments detached from larger shattered crystals (Fig. 4f). Olivine phenocrysts in mafic lavas and magmatic inclusions are usually larger (up to 2·5 mm) than in the andesitic and dacitic lavas. Grains in the magmatic inclusions typically form fractured, euhedral to subhedral polyhedra, although crystals with incomplete skeletal morphologies are not uncommon. Compositions of olivine phenocryst cores in all rock types range from Fo_{86} to Fo_{74}, although there is no systematic relationship between olivine and whole-rock compositions (Table 3). Rims of phenocrysts ($Fo_{83–71}$) are normally zoned up to 10 mol % Fo content relative to core compositions.

Forsterite contents of olivine phenocrysts are plotted versus the *mg*-number [100 Mg/(Mg + Fe^{2+})] of the enclosing rock in Fig. 5. Magmatic inclusions and lower-silica andesitic lavas (e.g. Gua13 and Gua9) have olivine core and rim compositions compatible with liquidus or near-liquidus nucleation at appropriate oxygen fugacities, followed by progressive growth of new crystals and rims with evolution of the liquid. In more silicic andesitic and dacitic lavas the cores of olivine phenocrysts are too Mg rich to have crystallized from liquids represented by their host whole-rock compositions. We suggest that the olivine grains in these samples (and possibly the lower-silica andesites) are xenocrysts derived from the magmatic inclusions because the ranges of core and rim compositions are nearly identical to the ranges for olivine phenocrysts in coexisting inclusions (Fig. 5). One silicic andesitic lava (Gua6) contains olivine with relatively low Fo contents that are compatible with equilibrium liquidus nucleation. However, it is likely that these grains are also xenocrysts because their compositions are identical to those of olivine crystals present in coexisting 'fractionated' magmatic inclusion Gua6.MI (Fig. 5).

Pyroxene

Clinopyroxene and orthopyroxene in andesitic and dacitic lavas occur as isolated phenocrysts, in coarse-grained glomerocrysts, and as groundmass microphenocrysts. Phenocrysts and grains in glomerocrysts are elongated to equant (<2 mm across), euhedral to subhedral, and may be either reversely or normally zoned. Orthopyroxene in the magmatic inclusions is rare and when present as a phenocryst phase it is usually jacketed by clinopyroxene. Orthopyroxenes are mainly hypersthenic and calcic pyroxenes are augitic.

The *mg*-numbers of clinopyroxene and orthopyroxene phenocryst cores and rims are plotted versus the FeO*/MgO of the host rock in Fig. 6. The *mg*-numbers of clinopyroxene are higher than those of coexisting orthopyroxene, implying early precipitation of clinopyroxene, followed by orthopyroxene. Clinopyroxene phenocryst cores in all samples are too Fe rich to have crystallized at liquidus con-

Table 3: Representative olivine point analyses

Sample:	14	13	9	9.MI	6	6.MI	21	21.MI	3A	3A.MI	12
SiO_2	37·06	39·04	39·62	38·69	39·00	38·90	39·75	39·24	39·47	39·91	38·69
FeO*	23·99	15·85	15·09	20·60	20·42	20·17	15·28	15·33	15·15	15·87	19·12
MnO	0·45	0·25	0·22	0·31	0·39	0·31	0·21	0·26	0·29	0·23	0·27
MgO	38·25	43·83	45·25	40·51	39·72	39·68	44·21	44·23	44·18	43·61	40·64
CaO	0·20	0·13	0·16	0·17	0·17	0·20	0·18	0·19	0·14	0·15	0·20
NiO	0·03	0·63	0·21	0·10	0·02	0·10	0·10	0·16	0·20	0·14	0·00
Total	99·98	99·73	100·55	100·38	99·72	99·36	99·73	99·41	99·43	99·91	98·92
mol% Fo	74·0	83·1	84·2	77·7	77·5	77·8	83·8	83·7	83·8	83·00	79·10

ditions in equilibrium with melts similar in composition to their host rocks. The low *mg*-numbers of the pyroxene in the magmatic inclusions can be explained either by nucleation of clinopyroxene under subliquidus conditions following liquidus crystallization of olivine, or by incorporation of xenocrystic pyroxene from more Fe-rich melts. Liquidus crystallization of olivine cannot account for the Fe-rich nature of the clinopyroxene in the andesitic and dacitic lavas, however, because in most or all of these samples the olivine crystals are xenocrysts. Instead,

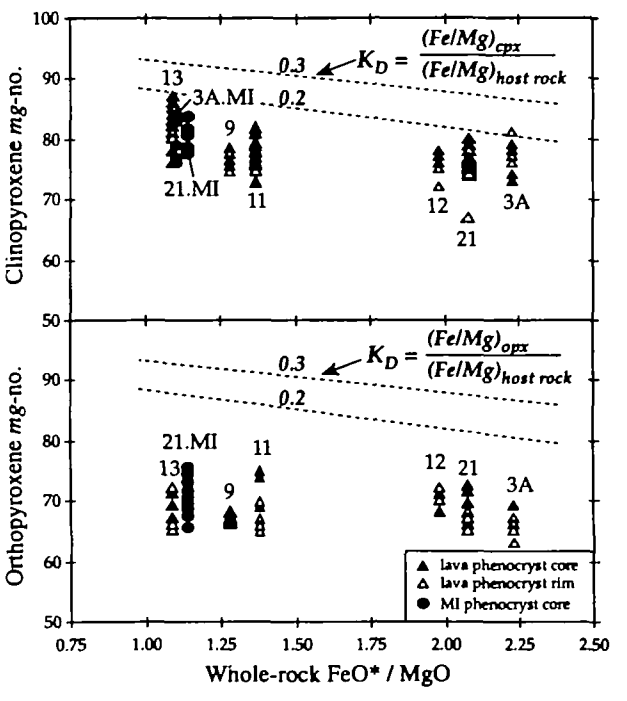

Fig. 6. Molar *mg*-numbers of clinopyroxene and orthopyroxene phenocrysts vs whole-rock FeO*/MgO. Lines represent equilibrium between minerals and whole-rock compositions. The lines were calculated as in Fig. 5 using equilibrium $^{Fe/Mg}K_{D\ min/liq}$ values of 0·20–0·30 (Grove *et al.*, 1982; Baker & Eggler, 1983).

the Fe-rich nature of the clinopyroxene phenocrysts probably reflects incorporation of a less evolved magma into host magma following pyroxene crystallization.

Figure 7 illustrates ternary compositions of pyroxene phenocryst cores and rims, and groundmass microphenocrysts in the magmatic inclusions and silicic lavas projected onto the temperature-contoured pyroxene quadrilateral (Lindsley, 1983). Pyroxene cores from the lavas have a limited compositional range of $Wo_{1-3}Fs_{26-34}En_{64-73}$ for orthopyroxene and $Wo_{39-42}Fs_{9-16}En_{43-52}$ for clinopyroxene. In addition, the differences between rim and core compositions of individual phenocrysts are usually not more than ~3 mol % En. There is no apparent compositional distinction between isolated phenocrysts and grains in glomerocrysts and, where analyzed, the cores of pyroxenes from the magmatic inclusions are similar to those in coexisting host lavas (Fig. 7).

Relative to phenocrysts, clinopyroxene groundmass microphenocrysts have lower Ca/(Ca + Mg + Fe) and generally higher Mg/(Mg + Fe) (Fig. 7). These grains are compositionally identical in all respects to groundmass augite in the magmatic inclusions, and considering the petrographic evidence for inclusion disaggregation presented above, they are probably derived from them. Supporting this interpretation are the Ti and Al contents and *mg*-numbers of the groundmass microphenocrysts in the lavas, which are generally higher than those for phenocryst cores and rims (Fig. 8). Experimental and petrologic investigations have demonstrated that partitioning of minor elements such as Ti and Al in pyroxene is strongly growth-rate dependent, whereas equilibrium partitioning of Ca, Mg, and Fe between pyroxene and melt may not be seriously affected by high cooling rates (Dungan & Brown, 1977; Grove & Bence, 1977; Gamble & Taylor, 1980; Schiffman

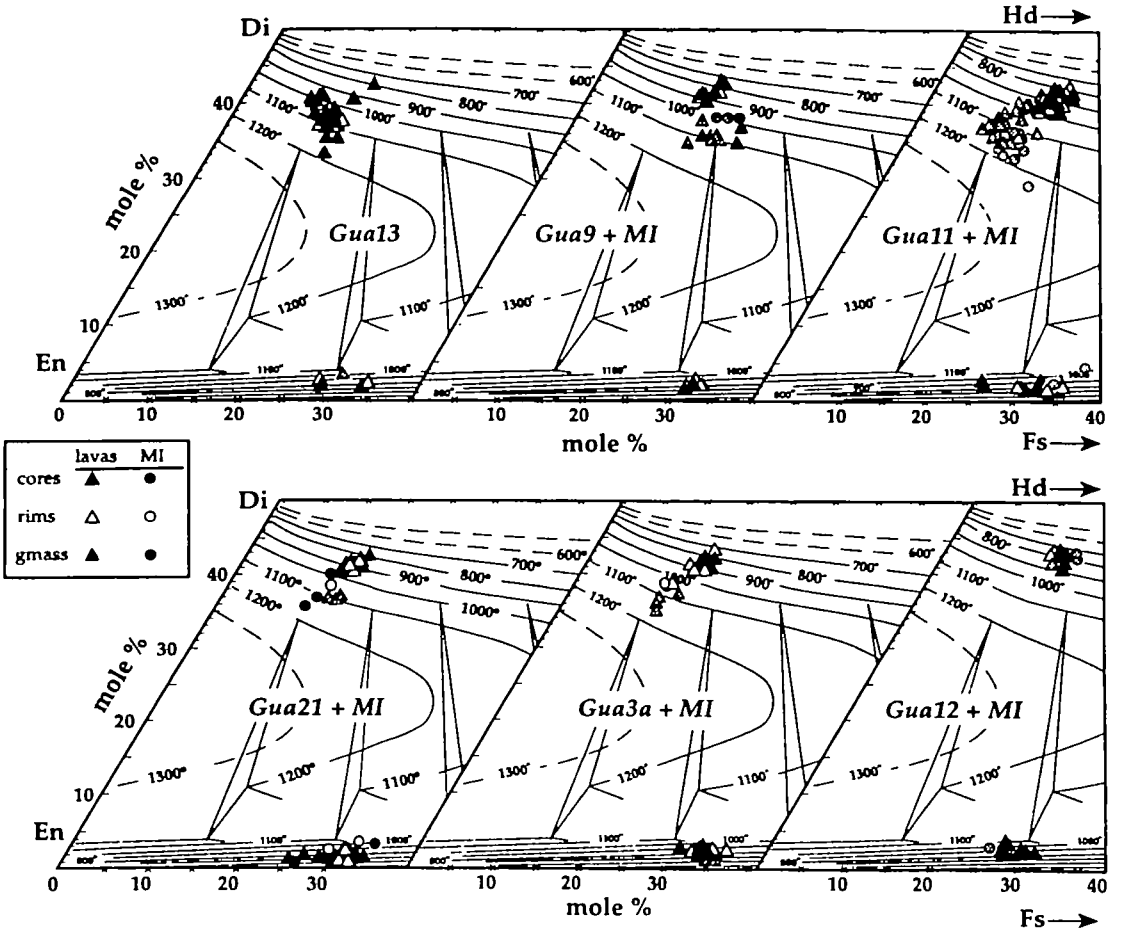

Fig. 7. Pyroxene compositions for Guadal volcanic rocks grouped according to individual lava flow and coexisting inclusions. Each point represents an analysis. Compositions recalculated according to Lindsley (1983) and plotted relative to isotherms determined by the same.

& Lofgren, 1982). In particular, high cooling rates favor crystallization of pyroxene with elevated Ti and Al contents relative to pyroxene in more slowly cooled rocks. The Mg-, Ti-, and Al-rich groundmass pyroxene in the andesitic and dacitic lavas therefore probably reflect crystallization in high-Mg inclusion-forming magmas at elevated cooling rates, followed by mechanical dispersal into host-forming andesitic and dacitic magma.

Fe–Ti oxide redox equilibria

Ti-rich magnetite is the most abundant oxide phase in the andesitic and dacitic lavas, although all samples also contain sparse, but ubiquitous ilmenite. Average compositions of three to five mineral pairs per sample with four to six analyses per grain are presented in Table 4. No analyses of oxides from the magmatic inclusions are reported because they are invariably exsolved, presumably owing to subsolidus cooling following incorporation and undercooling in the andesitic and dacitic magmas. Oxygen fugacities and equilibration temperatures calculated using the Fe–Ti oxide geothermometer of Ghiorso & Sack (1991) are presented in Table 4 and illustrated in Fig. 9. All samples used to calculate temperatures and oxygen fugacities are pristine, contiguous pairs with equilibrium Mg–Mn partitioning according to the criterion established by Bacon & Hirschmann (1988; Fig. 9).

The calculated redox equilibria for Guadal andesitic and dacitic lavas form a diffuse linear array that lies ~0·25–1 log units above the synthetic nickel–nickel oxide buffer curve. The ranges of temperature and oxygen fugacity are similar to those of many other arc-related andesitic and dacitic suites (Gill, 1981). Relative to other Quaternary volcanic centers in proximity to the Tatara–San Pedro complex, Guadal dacitic samples have Fe–Ti oxide redox equilibria similar to historic dacitic magmas erupted from Volcán Quizapu to the north of the complex, although they are slightly more reduced than dacitic

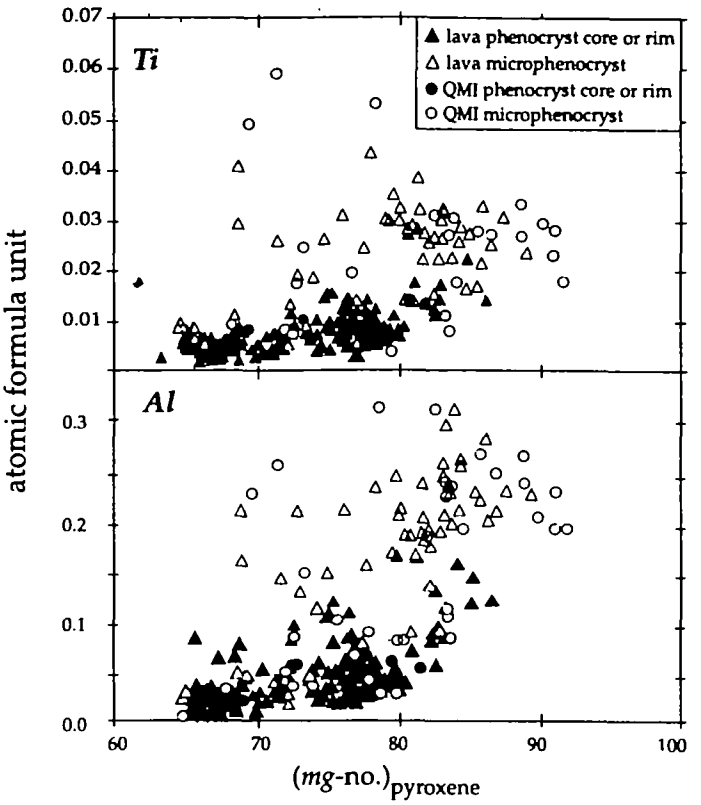

Fig. 8. Ti and Al atomic formula units (a.f.u.) of pyroxene phenocrysts and groundmass grains in Guadal lavas and magmatic inclusions vs whole-rock *mg*-number.

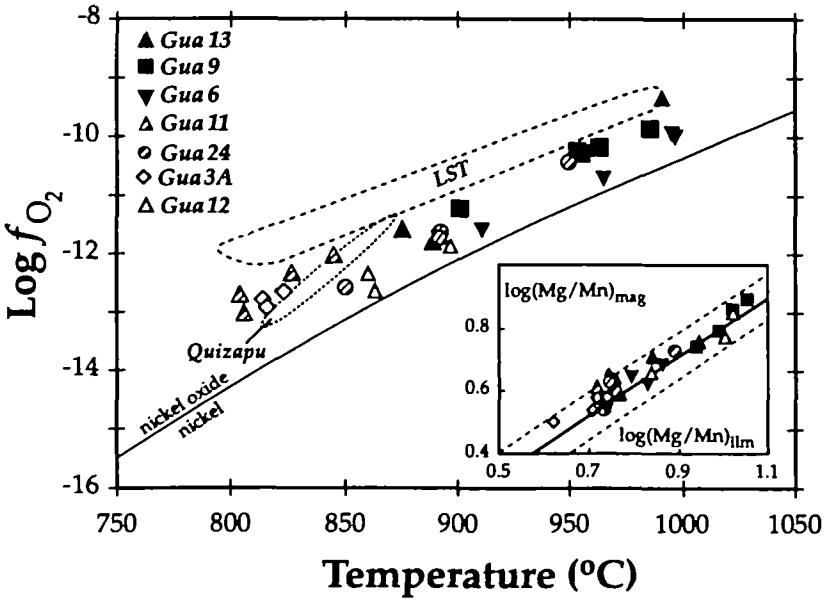

Fig. 9. Fe–Ti oxide estimates of temperature and oxygen fugacity in Guadal volcanic rocks determined by the model of Ghiorso & Sack (1991). Nickel–nickel oxide buffer curve from Heubner & Sato (1970). Fields for dacitic volcanic rocks from Volcán Quizapu (Hildreth & Drake, 1992) and unit S of the Loma Seca Tuff (LST; Grunder & Mahood, 1988) shown for reference. Inset shows atomic Mg/Mn of Guadal Fe–Ti oxides. Heavy continuous line is equilibrium line empirically determined by Bacon & Hirschmann (1988). Dashed lines show limits of $\pm 2\sigma$ error envelope.

Table 4: Average Fe–Ti oxide analyses and estimated temperatures

Sample:	Gua13	Gua9	Gua6	Gua11	Gua24	Gua3A	Gua12
Titanomagnetite							
SiO_2	0·12	0·09	0·09	0·07	0·06	0·06	0·08
TiO_2	10·57	12·45	14·13	8·62	11·77	8·85	12·53
Al_2O_3	1·68	1·62	1·65	1·16	1·76	1·25	1·88
Cr_2O_3	0·04	0·05	0·03	0·06	0·02	0·03	0·03
V_2O_3	0·62	0·50	0·49	0·56	0·48	0·51	0·54
FeO*	80·20	78·03	75·72	83·70	79·34	82·11	77·81
MnO	0·40	0·47	0·58	0·38	0·43	0·45	0·46
MgO	0·90	1·78	1·31	0·87	1·09	0·93	1·53
CaO	0·05	0·04	0·03	0·03	0·01	0·02	0·01
Total	94·58	95·02	94·03	95·44	94·97	94·20	94·87
Fe_2O_3	45·93	42·84	38·74	51·33	43·94	49·95	42·34
FeO	38·87	39·18	41·11	37·51	39·82	37·16	39·72
Total	99·18	99·01	98·15	100·58	99·40	99·20	99·11
Ilmenite							
SiO_2	0·02	0·02	0·03	0·07	0·02	0·01	0·02
TiO_2	43·16	44·73	45·68	45·52	45·61	45·35	47·13
Al_2O_3	0·19	0·18	0·17	0·10	0·14	0·11	0·14
Cr_2O_3	0·02	0·02	0·01	0·02	0·02	0·02	0·01
V_2O_3	0·50	0·42	0·41	0·40	0·40	0·42	0·43
FeO*	51·93	49·71	48·89	50·43	49·91	49·62	47·24
MnO	0·46	0·57	0·67	0·68	0·58	0·70	0·60
MgO	1·77	3·18	2·43	2·10	2·01	2·01	3·14
CaO	0·03	0·02	0·03	0·03	0·03	0·02	0·03
Total	98·07	98·85	98·31	99·35	98·72	98·26	98·74
Fe_2O_3	18·45	17·34	14·43	15·39	14·27	14·70	12·16
FeO	35·33	34·11	36·19	36·58	36·95	36·56	36·29
Total	99·91	100·59	100·03	100·89	100·03	99·91	99·95
T (°C) (G&S)	929	964	956	816	895	816	876
log f_{O_2}	−10·6	−10·1	−10·7	−12·7	−11·6	−12·9	−12·2
range T (°C)	876–991	953–986	912–996	804–845	850–950	814–823	860–896

Each analysis represents an average of at least three grains per sample with 3–5 analyzed points per grain. Temperature and oxygen fugacity calculated by the method of Ghiorso & Sack (1991).

ignimbrites erupted from the Calabozos caldera complex, which lies 50 km to the northeast (Fig. 9).

Plagioclase

Phenocryst compositional and textural types

Representative point analyses of plagioclase crystals in lavas and magmatic inclusions are presented in Table 5. Textures and zoning characteristics of phenocrysts in silicic lavas and magmatic inclusions investigated by the Nomarski contrast interference technique, and core to rim electron microprobe traverses, are illustrated in Fig. 10. Frequency histograms of plagioclase compositions, distinguished on the basis of phenocryst core, phenocryst rim, and groundmass microlite are shown in Fig. 11. Except for basaltic lava Gua14 and andesitic lava Gua13, ~90% of all plagioclase phenocrysts in the lavas and magmatic inclusions can be assigned to one of four textural and compositional types discussed below.

Table 5: Representative point analyses of plagioclase crystals by type

Sample:	13	13	11	11	12	12	11	11	12	12	3A	3A	11.MI	11.MI	21.MI	21.MI	3A.MI
Type:[1]	1c	1r	1c	1r	2c	2r	3c	3r	4c	4r	1gm	2gm	3c	3r	4c	4r	2gm
SiO_2	51·26	52·86	58·99	59·13	44·35	56·01	60·09	51·74	44·98	52·63	60·45	50·85	60·13	51·50	46·71	52·73	51·21
Al_2O_3	29·99	28·67	25·36	24·99	34·83	26·91	24·86	30·40	34·36	29·29	23·64	29·94	24·82	30·14	33·15	28·32	29·95
FeO*	0·69	0·89	0·28	0·35	0·49	0·51	0·33	0·74	0·41	0·79	0·42	0·91	0·21	0·83	0·45	0·95	0·84
MgO	0·12	0·08	0·00	0·01	0·04	0·05	0·01	0·03	0·01	0·05	0·02	0·01	0·03	0·03	0·01	0·05	0·05
CaO	13·11	11·93	7·06	6·82	18·94	9·53	6·61	12·89	17·85	12·03	7·49	13·53	6·89	13·26	18·22	12·92	13·18
Na_2O	3·94	4·77	7·46	7·24	0·80	5·83	7·19	4·04	1·46	4·49	6·99	3·76	7·40	3·94	1·47	4·23	3·64
K_2O	0·16	0·28	0·68	0·83	0·03	0·46	0·91	0·21	0·05	0·27	0·60	0·20	0·84	0·23	0·06	0·18	0·45
Total	99·27	99·48	99·83	99·37	99·48	99·30	100·00	100·05	99·12	99·55	99·61	99·20	100·32	99·93	100·05	99·38	99·22
mol%																	
An	64·17	57·08	33·03	32·62	92·70	46·21	31·92	63·05	86·90	58·79	35·91	65·79	32·37	64·16	87·04	62·20	65·47
Ab	34·88	41·32	63·19	62·65	7·10	51·12	62·87	35·73	12·83	39·68	60·65	33·03	62·91	34·53	12·70	36·80	31·88
Or	0·95	1·59	3·79	4·73	0·19	2·67	5·21	1·22	0·26	1·54	3·45	1·18	4·72	1·31	0·26	1·01	2·65

[1]Number refers to sample type discussed in text. Suffix c—core, r—rim, gm—groundmass.

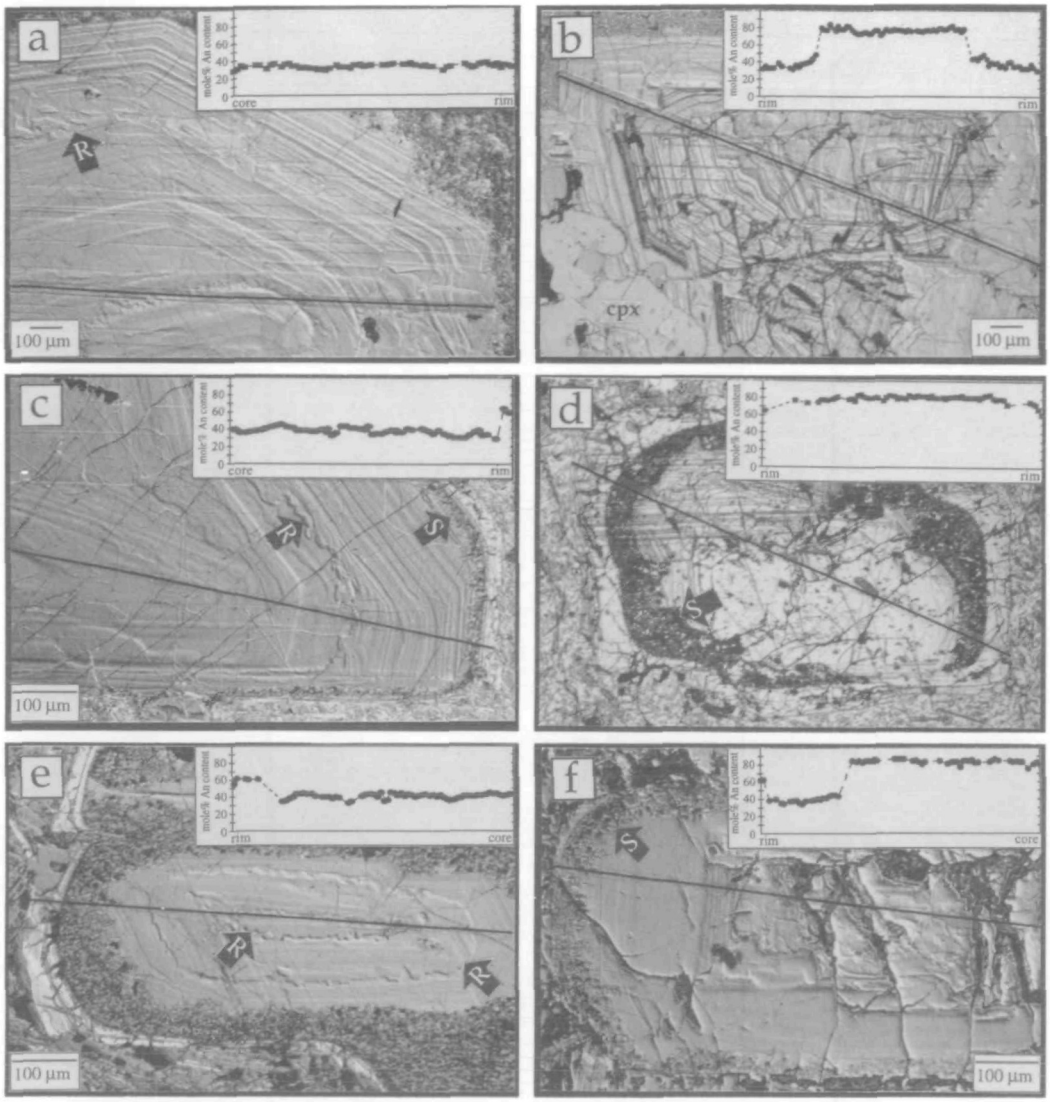

Fig. 10. Nomarski interference contrast images and core to rim electron microprobe traverses of plagioclase in Guadal lavas and magmatic inclusions. (a) Type 1 unzoned andesine phenocryst in dacitic lava (Gua21). [Note irregular resorption surface (R) that is not associated with significant jump in An content.] (b) Type 2 phenocryst in dacitic lava (Gua3A). Phenocryst has unzoned, highly calcic core followed by a major resorption surface associated with an abrupt drop in An content of 50–60 mol %, and succeeded by a euhedral andesine rim. [Note clinopyroxene (cpx; lower left) intergrown with plagioclase rim in glomerocryst.] (c) Type 3 phenocryst in andesitic lava (Gua9). Phenocryst has andesine core and texture similar to that of Type 1 phenocrysts surrounded by sieve-textured zone (S) containing sub-micrometer scale glass channels, which is mantled by thin (~10 mm), intermediate composition euhedral rim. (d) Type 4 phenocryst in andesitic lava (Gua9). Phenocryst has resorbed calcic core texturally and compositionally identical to those of Type 2, but with rim texture and composition identical to those of Type 3. Extent of sieved region corresponds to area of assimilated andesine mantle [see (f)]. (e) Type 3 phenocryst in magmatic inclusion (Gua3A.MI). (f) Type 4 phenocryst in magmatic inclusion (Gua21.MI).

Plagioclase relationships in Gua14 and Gua13 are discussed separately.

Type 1: Euhedral, unzoned to normally zoned, andesine phenocrysts (An_{50-30}; Fig. 10a). The interior regions of these crystals always display one or a few resorption surfaces associated with minor jumps in An content (<3 mol %). These surfaces presumably indicate periods of dissolution and volume loss. The bulk of the plagioclase phenocrysts in the andesitic and dacitic lavas display these zoning and textural characteristics. Type 1 phenocrysts occur in glomerocrysts or, more commonly, as isolated phenocrysts. They are never present in the magmatic inclusions.

Type 2: An-rich crystals with unzoned, mainly bytownite cores (An_{70-94}) surrounded by euhedral andesine rims identical in composition to the cores and rims of Type 1 phenocrysts (An_{50-30}; Fig. 10b). The interfaces between the An-rich cores and

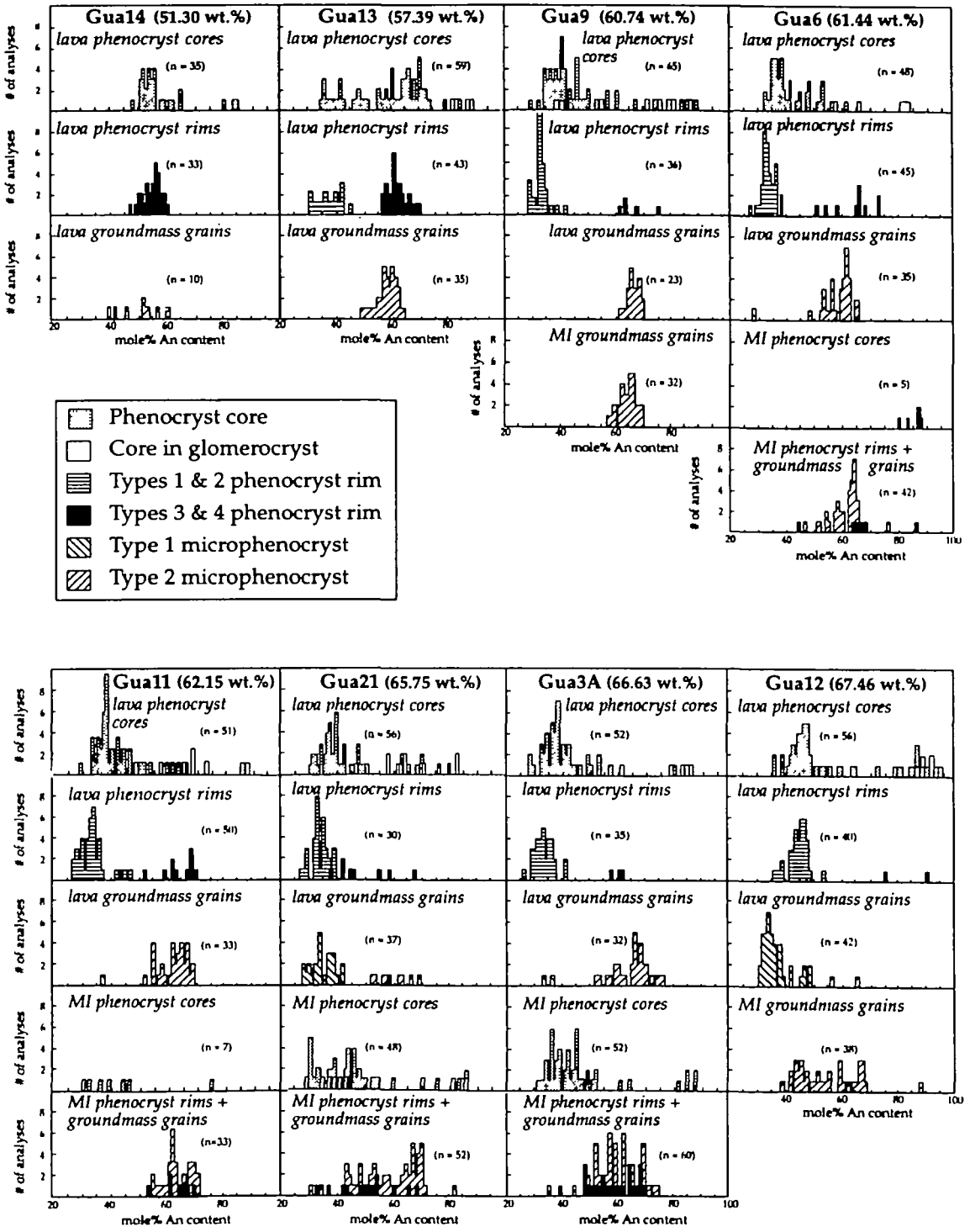

Fig. 11. Frequency histograms of plagioclase core, rim, and groundmass compositions for Guadal lavas and magmatic inclusions (MI). Magmatic inclusion plagioclase is illustrated in same column as coexisting host lava. *n* is number of analyses, i.e. number of individual crystals analyzed. SiO_2 contents of lava flows indicated next to labels. The following should be noted: (1) the similarity between lava and inclusion plagioclase core compositions (e.g. Gua6, Gua11, Gua21, Gua3A); (2) the extremely An-rich nature of a few plagioclase cores (up to An_{94}), especially those in glomerocrysts, from all samples; (3) the similarity between Type 3 and 4 phenocryst rims in host lavas and inclusions; (4) the similarity between Type 2 host lava microphenocrysts and Type 2 inclusion microphenocrysts; and (5) the relatively Na-rich nature of Type 1 and 2 phenocryst rims, their compositional similarity to Type 1 microphenocrysts, and their slight normal zoning relative to the bulk of phenocryst cores.

andesine rims are rounded to planar, and they are typically conformable to previous growth zones or resorption surfaces. These relations are similar to descriptions of the 'smooth' interfaces produced in experiments by Tsuchiyama (1985), which result from the introduction of calcic plagioclase into melt more sodic than the equilibrium composition. Type 2 phenocrysts are typically more equant and larger than Type 1 phenocrysts, and they are particularly abundant in the coarse-grained glomerocrysts, although isolated crystals are also common (Figs 4d and 11). They never occur in the magmatic inclusions.

Type 3: Phenocrysts with andesine cores (An_{50-30}) and textural characteristics identical to those of Type 1 phenocrysts, but that are surrounded by sieve-textured zones (1–200 mm across) containing concentrated sub-micrometer scale interconnected glass channels, which in turn are mantled by thin (10–100 mm across), intermediate composition (An_{50-70}), euhedral rims (Fig. 10c, e). The sieve-textured zones are analogous to the 'dusty' zones, and the sieved zone–core interfaces are similar to the 'rough' interfaces produced in the partial dissolution experiments of Tsuchiyama (1985). Both result when sodic plagioclase is admixed into a high-temperature melt more calcic than the equilibrium composition. In Type 3 phenocrysts the sieve-textured zones always occur rimward of the resorption surfaces present in Type 1 phenocrysts. Type 3 plagioclase phenocrysts occur in both host lavas and magmatic inclusions.

Type 4: These crystals are in essence Type 2 phenocrysts surrounded by Type 3 rims. For example, the Type 4 phenocryst illustrated in Fig. 10f has a composite core composed of an unzoned An-rich interior and an andesine mantle. This core is in turn surrounded by a sieve-textured zone and a thin, intermediate-composition euhedral rim. In some Type 4 crystals the interior andesine mantles have completely reacted so that the An-rich cores are in direct contact with the sieved zones (Fig. 10d). Type 4 plagioclase phenocrysts occur in both lavas and magmatic inclusions as isolated phenocrysts and in glomerocrysts. In rare cases, and only in the magmatic inclusions and basaltic lavas, An-rich cores are in direct contact with the intermediate composition rims, without an intervening sieved zone. In these particular crystals there is no evidence that an andesine overgrowth ever mantled the An-rich core.

Summary of plagioclase phenocryst compositional–textural types

The presence of plagioclase phenocrysts in the andesitic and dacitic lavas with cores that are either andesine (Types 1 and 3) or An rich (Types 2 and 4), and rims that are either andesine (Types 1 and 2) or intermediate (Types 3 and 4), imparts crudely bimodal distributions to the histograms of phenocryst core and rim compositions (Fig. 11). In these spectra the andesine peak dominates. Importantly, the frequency spectrum of plagioclase phenocryst cores in the magmatic inclusions usually matches the spectrum of its coexisting host lava (e.g. Gua11, Gua21 and Gua3A). An exception is the frequency distribution for sample Gua6.MI, which reflects only An-rich cores. The relationships discussed are still valid for this sample, however, because, although originally present, we were unable to obtain analyses for any andesine phenocryst cores because all are now totally sieved. The main difference between plagioclase phenocrysts in the lavas and inclusions is thus in the rim compositions; phenocrysts in the lavas have rims that are either andesine or intermediate, whereas rims of inclusion plagioclase are only of the intermediate composition variety (Fig. 11). Lava phenocrysts may also either possess or lack outward sieve-textured regions, whereas nearly all inclusion phenocrysts are sieve-textured slightly inboard of the crystal rim. Because of these sieved regions we do not consider the Type 3 and 4 phenocrysts as demonstrating simultaneous reverse and normal zoning toward an intermediate composition, as they have not experienced a continuous growth history. This is an important distinction because apparently similar zoning patterns together with bimodal core spectra are often cited as evidence for simple mixing of mafic and silicic magmas to form a continuous spectrum of intermediate composition magmas (e.g. Graham & Worthington, 1988; Tormey *et al.*, 1995). However, as discussed below, our data and textural observations are more consistent with a complex history involving discrete magma mixing and commingling events.

Exceptions to the general relationships discussed above are exhibited by plagioclase in basaltic lava Gua14 and andesitic lava Gua13. In these samples the core and rim compositions are more calcic (An_{50-70}) than the bulk of the plagioclase phenocrysts in the inclusions and andesitic and dacitic lavas, although zoning profiles are similar to Type 1 phenocrysts. In addition, Gua13 contains a subpopulation of 'true' Type 1 phenocrysts (Fig. 11).

Groundmass plagioclase compositional types

Groundmass microphenocrysts in the lavas can also be subdivided into two compositional groups. Type 1 microphenocrysts have a narrow compositional range (An_{40-27}) similar to, or slightly more albitic

than rims of Type 1 and 2 phenocrysts. This type of microphenocryst occurs mainly in dacitic lavas (Fig. 11). Type 2 microphenocrysts have a narrow compositional range (An_{50-70}) identical to that of quench microphenocrysts in coexisting inclusions (Fig. 11). Relative to phenocryst rim compositions, they are distinctly more Ca rich than the rims of Type 1 and 2 phenocrysts, although they are similar to the rims of Types 3 and 4. Type 2 microphenocrysts occur mainly in andesitic lavas and dacitic lava Gua3A, although all samples contain at least a small percentage. In dacitic lavas Type 2 microphenocrysts appear to be concentrated in regions adjacent to magmatic inclusions, whereas in andesitic lavas they are distributed more or less randomly throughout the groundmass.

Plagioclase–melt equilibria

Figure 12a shows the *ca*-numbers [= Ca/(Ca + Na)] of Guadal whole-rock compositions plotted versus the average *ca*-numbers of plagioclase phenocrysts with andesine (Type 1 and 3) and An-rich cores (Type 2 and 4). Figure 12b shows *ca*-numbers of the groundmass glass analyses (Table 2) plotted versus average values for: (a) Type 1 and 2 phenocryst rims, (b) Type 3 and 4 phenocryst rims outboard of the sieve-textured zones, (c) Type 1 lava groundmass microphenocrysts, (d) Type 2 lava groundmass microphenocrysts, and (e) magmatic inclusion groundmass microphenocrysts and phenocryst rims. Items in (a), (b), and (c) have been grouped because of similar compositional features. Also illustrated in Fig. 12 are curves approximating equilibrium partitioning of Ca and Na between plagioclase and liquid. For values of K_D^{Ca-Na} ($= X_{Ca}^{plag} \cdot X_{Na}^{liq}/X_{Na}^{plag} \cdot X_{Ca}^{liq}$) we illustrate a range of values from 2 to 5·5 following the experimental studies of Baker & Eggler (1987), Housh & Luhr (1991), Sisson & Grove (1993), and Panjasawatwong *et al.* (1995). Collectively, these studies demonstrate that: (1) K_D^{Ca-Na} values are largely between 2 and 5·5 for basaltic to dacitic melts crystallized under H_2O-undersaturated to H_2O-saturated conditions at varying melt–H_2O contents, (2) for H_2O-saturated melts above 2 kbar, K_D^{Ca-Na} values increase drastically with increasing melt–H_2O contents, and (3) for H_2O-undersaturated melts with *ca*-numbers $<0·5$, equilibrium K_D^{Ca-Na} values are between 2 and 4 and appear to be independent of melt–H_2O content.

Type 1 and 3 plagioclase phenocrysts. With the exception of dacitic lava Gua12, cores of Type 1 plagioclase phenocrysts in the silicic lavas are too Na rich to have crystallized from liquids compositionally similar to their host whole rocks (Fig. 12a). Furthermore, in most lavas these crystals are compositionally similar so that the apparent degree of disequilibrium increases with increasing whole-rock *ca*-number, assuming constant K_D^{Ca-Na}. These results cannot be explained by nucleation of plagioclase under subliquidus conditions following crystallization and accumulation of clinopyroxene because the small amount of augite in the lavas is insufficient to account for the low *ca*-numbers of the Type 1 cores, and there is no correlation between the apparent degree of plagioclase–whole-rock disequilibrium and modal clinopyroxene. More likely, the high *ca*-numbers of the liquids containing andesine phenocrysts reflect disaggregation of largely quenched magmatic inclusions and contamination of silicic magmas following nucleation and growth of the plagioclase phenocrysts. We suggest that the inclusions commingled rather than mixed with the silicic magmas because: (1) rims of the Type 1 phenocrysts and Type 1 groundmass microphenocrysts in the silicic lavas have compositions that are appropriate for equilibrium crystallization from surrounding quenched groundmass liquid; whereas (2) Type 2 groundmass microphenocrysts in the lavas have compositions that are too Ca rich to have crystallized from surrounding groundmass, although they are similar to groundmass microphenocrysts in the magmatic inclusions (Fig. 12b). Because the Type 2 microphenocrysts are less abundant in dacitic than andesitic lavas, the mass of inclusions disaggregated into the silicic lavas appears qualitatively to decrease with increasing SiO_2 contents of the lavas.

Type 3 plagioclase phenocrysts are present in the silicic lavas and magmatic inclusions, and in both occurrences they have cores that are compositionally identical to the cores of Type 1 phenocrysts. However, unlike the Type 1 phenocrysts, Type 3 crystals possess sieve-textured zones that are mantled by rims identical in composition to quench microphenocrysts in the magmatic inclusions. We explain these features by initial precipitation of Type 3 phenocryst cores in silicic magma, followed by mixing into the mafic inclusion-forming magmas, assimilation, and precipitation of an intermediate composition rim. The implications of this interpretation are twofold. First, it indicates that the magmatic inclusions are blended hybrids formed by mixing of plagioclase-saturated dacitic magma and basaltic magma. Second, because Type 3 phenocrysts are in the silicic lavas, it indicates that following initial precipitation in dacitic magma, some andesine plagioclase phenocrysts experienced a transient history in the hybrid magmas before subsequently returning to the silicic magmas during

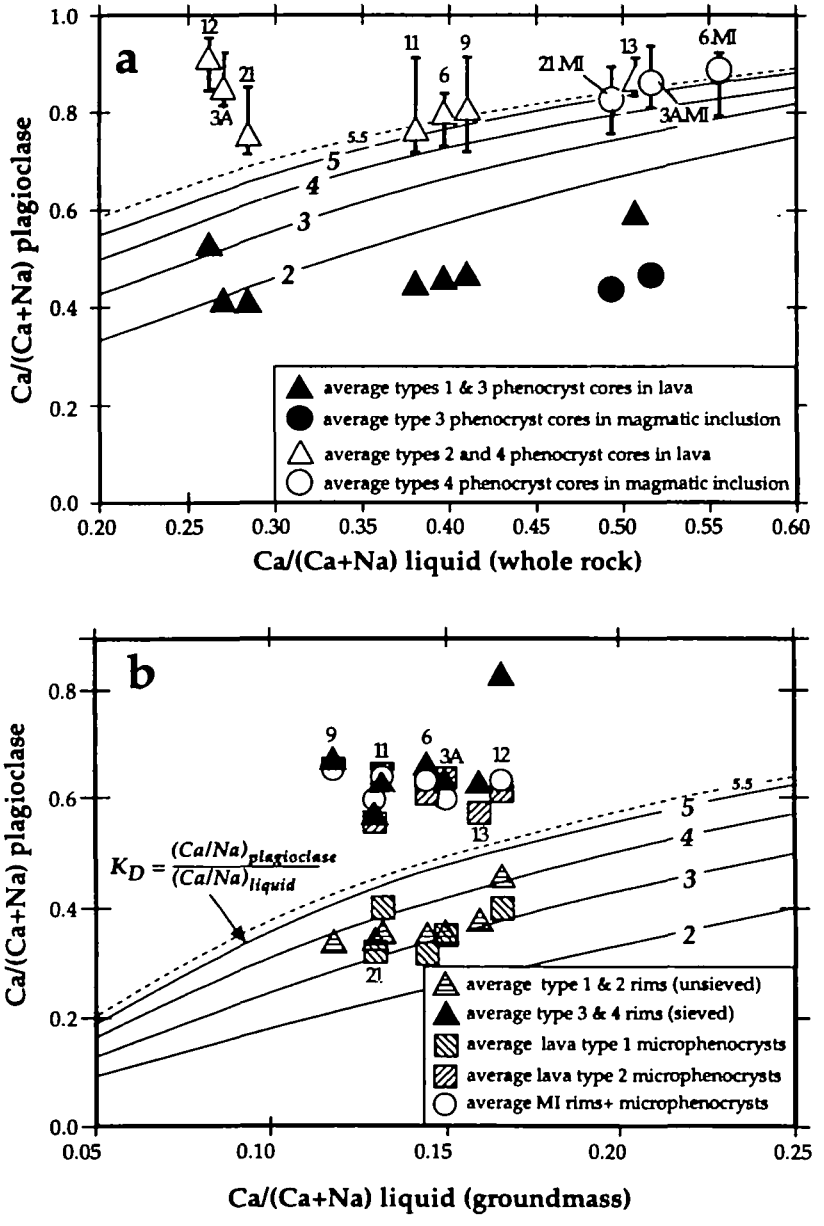

Fig. 12. (a) *ca*-numbers for Guadal whole-rock compositions plotted vs average *ca*-number of plagioclase phenocrysts with andesine (Types 1 and 3) and An-rich (Types 2 and 4) cores. Vertical bars on Type 4 symbols give the range of compositions in individual samples. (b) *ca*-numbers of host-rock groundmass plotted vs average values for: (1) Type 1 and 2 phenocryst rims; (2) Type 3 and 4 phenocryst rims; (3) lava groundmass microphenocrysts; and (4) magmatic inclusion groundmass microphenocrysts. The curves in both figures represent equilibrium values of $^{Ca/Na}K_{D\,min/liq}$ for hydrous melts based on experimental studies discussed in text.

inclusion disaggregation. Clynne (1996) has recently suggested an analogous model of mixing followed by commingling to explain geochemical and petrographic features of andesitic and dacitic volcanic rocks erupted in 1915 from Lassen Peak, California. Importantly, disaggregation of the inclusions at Cordón El Guadal must have occurred at the onset of, or just before eruption of the silicic magmas because the Type 3 phenocryst rims are unresorbed and lack the more albitic overgrowths expected if sufficient time had existed for equilibration with the silicic magmas.

Type 2 and 4 plagioclase phenocrysts. Plagioclase phenocrysts with extremely anorthitic compositions (up to An_{100}) and flat zoning profiles are common constituents of subduction-related high-Al basaltic lavas (e.g. Arculus & Wills, 1980; Brophy, 1986; Beard & Borgia, 1989). It is also becoming apparent

that plagioclase phenocrysts with similar An-rich cores form a minor, but common component of many calc-alkaline andesitic and dacitic lavas (e.g. Gerlach & Grove, 1982; Beard, 1986; Gerlach *et al.*, 1988; Brophy, 1990; Stamatelopoulou-Seymour *et al.*, 1990; Wallace & Carmichael, 1994; Tomiya & Takahashi, 1995; this study). As discussed by Sisson & Grove (1993) and Panjasawatwong *et al.* (1995), the origin of the An-rich phenocrysts must involve crystallization from melts with either extremely high CaO/Na_2O (>8) or high H_2O contents (~6 wt %), or, more likely, both. In the silicic examples most workers attribute the presence of An-rich phenocrysts to mixing evolved liquids with primitive basaltic magmas, although Wallace & Carmichael (1994) have suggested that for Mexican volcanic rocks the mafic mixing endmember was andesitic.

We interpret the An-rich Type 2 and 4 phenocryst cores in Guadal andesitic and dacitic lavas to have initially precipitated from refractory, possibly H_2O-rich, mafic magmas at elevated pressure. In dacitic lavas the cores of all Type 2 and 4 phenocrysts are much too calcic to have crystallized in equilibrium with liquids similar to their host whole-rock compositions at any H_2O content (Fig. 12a). Furthermore, although average compositions of Type 2 and 4 cores are appropriate for crystallization in Guadal andesitic or more mafic magmas, provided they were H_2O rich and H_2O saturated, the most An-rich grains in every sample are too calcic to have precipitated in any magma erupted in the Tatara–San Pedro Complex (Fig. 12a). Data from the experiments of Sisson & Grove (1993) indicate that the most An-rich plagioclase grains analyzed in the Guadal andesitic and dacitic lavas (An_{94}) could have initially crystallized from a melt with a *ca*-number of 0·77, assuming that the melt was both H_2O rich (e.g. 6%) and H_2O saturated. For comparison, the most primitive magma in the Guadal suite (Gua1MI; Davidson *et al.*, 1988) has a *ca*-number of 0·62, and the most primitive magma erupted during the entire 1 Ma history of the volcanic complex is 0·68 (M. A. Dungan, unpublished data, 1996). To precipitate An_{94} plagioclase from a melt with a H_2O content <6%, or at H_2O-undersaturated conditions, the *ca*-number of the melt must be considerably higher than 0·77 because H_2O appears to exert a strong control on plagioclase An contents only under saturated conditions (Panjasawatwong *et al.*, 1995). The evidence for crystallization of Type 2 and 4 phenocryst cores from refractory, possibly H_2O-rich, mafic melts thus suggests crystallization at elevated pressures owing to (1) the strong and well-known pressure dependence of H_2O solubility in magmas and (2) the absence of such melts in the Tatara–San Pedro Complex.

The compositional evidence for precipitation of the Type 2 and 4 phenocryst cores at elevated pressure from refractory mafic magmas and their common textural occurrence in glomerocrysts suggest that they represent fragments of mafic to ultramafic plutonic rocks crystallized at mid- to lower-crustal depths. Plagioclase with compositionally similar calcic cores and textural relationships are common in basal cumulate sequences of exposed deep crustal magma chambers beneath arc volcanoes (e.g. Beard, 1986; DeBari & Coleman, 1989). In these exposures, An-rich plagioclase occurs as a late crystallizing phase along with early Mg-rich olivine (Fo_{86-92}) and Mg- and Al-rich clinopyroxene (En_{40-48}; e.g. DeBari & Coleman, 1989). Intriguingly, in the Guadal samples the glomerocrysts in which the An-rich plagioclase cores occur consist solely of plagioclase or plagioclase complexly intergrown with low-Mg augite, orthopyroxene, or both. Wallace & Carmichael (1994) attributed a similar association of An-rich plagioclase with evolved augite and orthopyroxene in glomerocrysts from Mexican volcanic rocks to indicate crystallization in hydrous andesitic magmas. However, it is noteworthy that in the Guadal glomerocrysts the pyroxene crystals are intergrown exclusively with the andesine rims of the Type 2 crystals and not with their An-rich cores (Fig. 10b). Our interpretation is that the pyroxene crystals precipitated along with the andesine rims following entrainment of the An-rich plagioclase fragments into silicic magma bodies. We can only speculate as to how the deep-crustal cumulate fragments became incorporated into the silicic magmas and why they initially consisted solely of plagioclase clusters lacking mafic silicate phases. Perhaps they represent refractory solids retained from zones of crustal melting and silicic magma production. In this case, their presence may reflect a density fractionation process wherein buoyant plagioclase is suspended in ascending residual liquids, whereas fragments containing more dense mafic phases are selectively retained in deep crustal differentiation zones (e.g. Crawford *et al.*, 1987).

An alternative explanation is that the An-rich plagioclase cores represent xenocrysts derived from mixing plagioclase-bearing basaltic magmas into the silicic magmas. The principal lines of evidence against this hypothesis are as follows. First, most plagioclases in the andesitic and dacitic lavas are Type 1 phenocrysts with flat or normal zoning profiles. Absence of reverse zoning in these phenocrysts indicates that the silicic melts were little affected by processes such as mixing with mafic magmas. Second, Type 2 phenocrysts have rims that are similar to or slightly more albitic than the cores of

most Type 1 phenocrysts (Fig. 11). Thus, the silicic melts did not become more mafic at the time the Type 2 phenocrysts were entrained. Third, although the core compositions differ markedly, compositional and textural features of Type 2 and 4 phenocryst rims are identical to those of Type 1 and 3 phenocryst rims, respectively. Taken together, these relations suggest that the Type 2 and 4 phenocrysts record a similar petrogenetic history to the Type 1 and 3 phenocrysts. The difference, however, is that the An-rich cores were derived from zones of crustal melting rather than precipitating directly from the silicic melts. Finally, although basaltic lavas in the Guadal sequence (e.g. Gua14; Fig. 11) also contain plagioclase with similar An-rich cores, these crystals compose only a very small percentage (<10%) of the total number of phenocrysts in these samples. Most phenocrysts in Guadal basaltic lavas have cores of An_{50-60}, compositions that are relatively rare in the andesitic and dacitic lavas.

ESTIMATION OF PRE-ERUPTIVE TEMPERATURES AND MELT–H_2O CONTENTS

Pyroxene geothermometry

Average analyses of coexisting orthopyroxene and clinopyroxene phenocryst rims from andesitic and dacitic lavas are presented in Table 6 together with temperatures calculated by the methods of Wood & Banno (1973), Wells (1977), and Kretz (1982). Average temperatures calculated by the three methods range from 965 to 905°C for all samples, with values for dacitic lavas slightly lower than those for andesitic lavas (Fig. 13a). Projection of the pyroxene analyses in Fig. 7 (Lindsley, 1983) suggests temperatures between 800 and 1000°C for pyroxene cores and rims in the andesitic and dacitic lavas, except for those in the lowest silica andesitic lava (Gua13), for which it suggests temperatures between about 1000 and 1100°C.

Fe–Ti oxide geothermometry

Average Fe–Ti oxide equilibration temperatures of the andesitic and dacitic lavas are in several samples (e.g. Gua11, Gua3a, Gua12) substantially lower (<100°C) than estimates derived from clinopyroxene geothermometry, and oxide pairs from many samples yield a wide range in temperatures (≤115°C; Fig. 13a; Table 4). The large range in estimated temperatures for many lavas precludes equilibrium growth of oxide phases from slowly cooled, progressively differentiated magma bodies because of rapid cation diffusivities in oxide phases. Instead, they may reflect commingling and partial re-equilibration of oxide phases derived from relatively high- and low-temperature magmas, conceivably just before or during an eruptive event to inhibit complete re-equilibration (e.g. Nakamura, 1995). Nevertheless, variations in average Fe–Ti oxide temperatures with bulk lava compositions are similar to the pyroxene estimates in that oxide pairs from andesitic lavas typically yield higher estimates than those from dacitic lavas. For example, apart from sample Gua11, which has anomalously low calculated temperatures, Fe–Ti oxide pairs in andesitic samples yield temperatures that range from 996 to 876°C. Those from dacitic lavas yield a range of slightly larger magnitude, but which is shifted to lower values (950–814°C). The net effect is that combined averages for the two methods in a general way show an inverse correlation with SiO_2 (Fig. 13a).

Melt–H_2O contents

Because the andesine rims of Type 1 and 2 plagioclase phenocrysts in the andesitic and dacitic lavas appear to record pre-eruptive equilibrium (e.g. Fig. 12b), we have used their compositions along with the temperatures estimated from pyroxene rim and Fe–Ti oxide thermometry to calculate ranges in melt H_2O contents using the model of Housh & Luhr (1991; Fig. 13b; Table 2). These estimates are based on $P_{Total} = 2$ kbar. Differences between average melt–H_2O contents calculated from the independent anorthite and albite exchange reactions are generally low (mean ~0·3 wt % H_2O) and provide additional support for equilibrium between groundmass liquid and Type 1 and 2 phenocryst rims. Ranges in calculated melt–H_2O contents for most samples are large (1–4 wt %), however, because the calculated values are sensitive to temperature as well as groundmass and plagioclase compositions, and all samples yield relatively large ranges in temperature estimates from the various methods discussed above (Fig. 13c).

Nonetheless, H_2O contents calculated from the average temperature estimates appear to increase from ~1·5 to ~3 wt % as SiO_2 increases from 57 to 67 wt % (Fig. 13b). It is difficult to be certain if this trend represents a meaningful increase in melt–H_2O content with differentiation, or if it reflects the strong dependence of the calculated values on temperature. In detail, the trend for variation of melt–H_2O content with bulk lava SiO_2 is nearly a mirror image of the trend for temperature vs SiO_2 (Fig. 13a,b). This suggests that the increasing H_2O contents may simply reflect the effect of decreasing

Table 6: Average pyroxene rim analyses and estimated temperatures

	Gua13	Gua9	Gua11	Gua21	Gua3A	Gua12
Orthopyroxene						
SiO_2	53·53	53·53	52·98	53·27	53·47	54·53
TiO_2	0·21	0·18	0·17	0·15	0·05	0·22
Al_2O_3	0·75	0·58	0·49	0·50	0·45	0·84
FeO*	20·07	20·57	20·87	20·42	20·71	17·50
MnO	0·95	1·05	1·14	1·13	1·14	0·94
MgO	23·20	23·31	22·94	22·95	22·52	24·92
CaO	1·31	1·16	1·11	1·13	1·08	1·20
Na_2O	0·00	0·03	0·01	0·02	0·10	0·03
Total 100·04	100·41	99·70	99·58	99·52	100·20	
mol %						
Wo	2·62	2·40	2·25	2·33	2·52	2·45
En	65·56	65·27	64·72	65·15	64·29	69·97
Fs	31·82	32·32	33·03	32·53	33·19	27·58
Clinopyroxene						
SiO_2	50·13	52·82	52·10	52·60	51·89	52·84
TiO_2	0·95	0·29	0·34	0·03	0·40	0·45
Al_2O_3	3·97	1·24	1·37	1·04	1·92	2·02
FeO*	8·95	9·20	9·10	8·82	8·33	8·22
MnO	0·26	0·54	0·54	0·55	0·45	0·40
MgO	14·96	14·51	14·5	14·53	14·52	14·67
CaO	20·63	20·87	21·09	21·31	21·27	21·19
Na_2O	0·32	0·42	0·4	0·39	0·37	0·38
Total	100·16	99·90	99·44	99·26	99·15	100·17
mol %[1]						
Wo	39·27	42·46	42·17	42·89	42·93	43·38
En	48·12	43·07	44·17	43·75	44·16	43·09
Fs	12·61	14·47	13·66	13·36	12·92	13·53
T (°C) K[2]	935	920	880	860	850	895
T (°C) WB[3]	955	930	915	910	915	950
T (°C) W[4]	1000	965	950	940	950	965
Average *T* (°C)	965	940	915	905	905	935

[1]Ternary components calculated following the method of Lindsley (1983).
Temperatures calculated following the methods of [2]Kretz (1982), [3]Wood & Banno (1973), and [4]Wells (1977).

temperature on the calculated values. Moreover, as the *ca*-numbers of the Type 1 and 2 plagioclase rims and groundmass glasses in all samples are broadly similar and do not vary systematically with bulk lava SiO_2 (Table 2), there is no *a priori* reason to suspect that pre-eruptive H_2O contents of the melts varied in a systematic manner. Finally, although the relative positions of the curves in Fig. 13c imply a small range in pre-eruptive melt–H_2O contents among the samples considered ($\leqslant 1$ wt %), they demonstrate that the variation is not correlated with bulk lava SiO_2 content. The relatively low calculated average H_2O contents for all bulk compositions are, however, consistent with the absence of amphibole in these samples and the lack of evidence for explosive volcanic activity associated with eruption of the Guadal lavas (Luhr, 1992).

We suggest that the trend of increasing temperature (and hence decreasing calculated melt–H_2O contents) with decreasing SiO_2 reflects under-

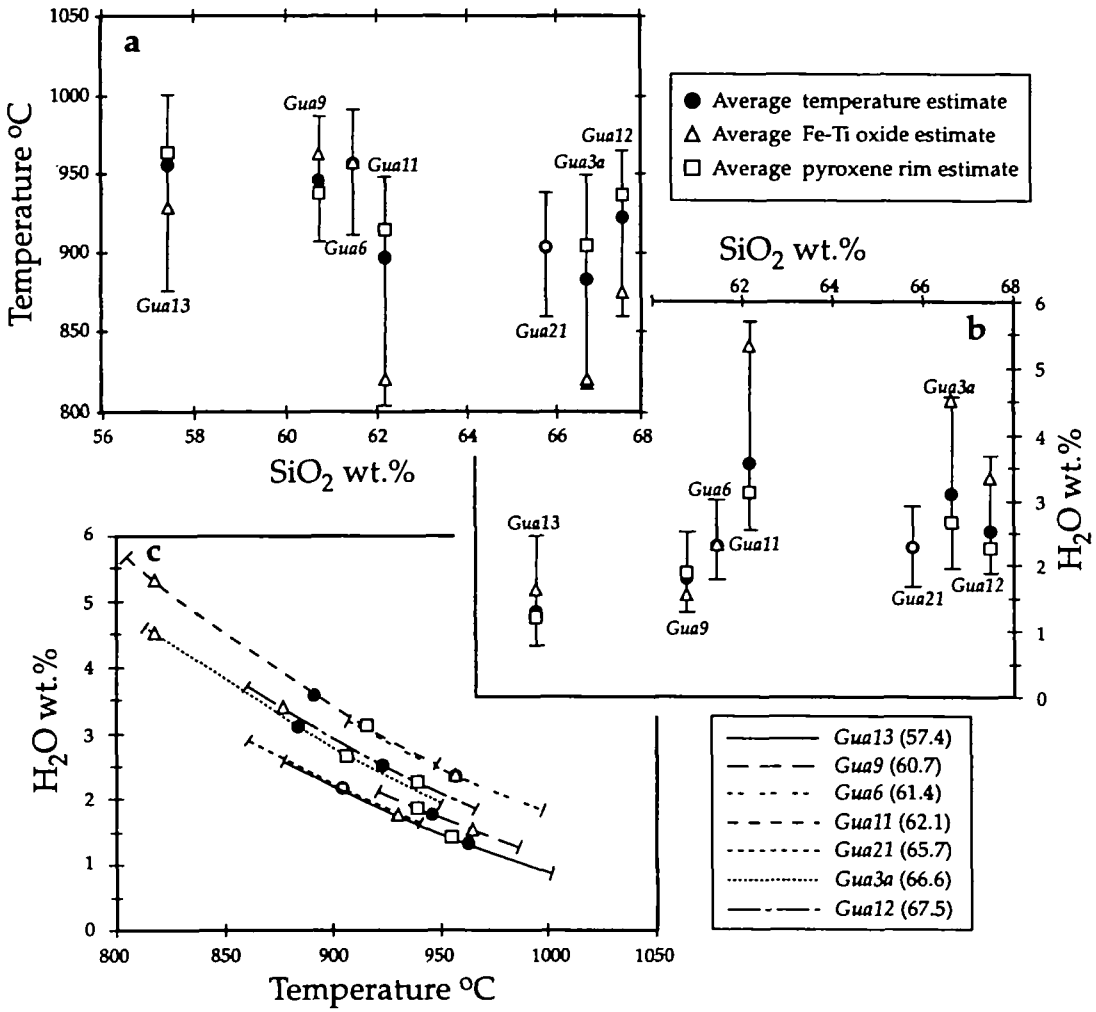

Fig. 13. (a) Temperatures calculated by the methods discussed in the text vs whole-rock SiO_2 of Guadal andesitic and dacitic lavas. Vertical bars give the range of calculated temperatures for individual samples. (b) Pre-eruptive melt-water contents for andesitic and dacitic lavas using the model of Housch & Luhr (1991), $P_{Total} = 2$ kbar, the temperature estimates illustrated in (a), and groundmass and plagioclase rim analyses (Table 2). (c) Variation in calculated melt-water contents with range of temperatures estimated for individual lavas. Legend at right gives SiO_2 content of lavas.

cooling, crystallization, and disaggregation of increasing amounts of largely solidified basaltic andesitic magma in dacitic or rhyolitic melts following plagioclase rim crystallization. Undercooling and disaggregation of basaltic andesitic magma in silicic magma should shift temperature estimates to higher values as heat is released and high-temperature phases are dispersed into the magma chambers. In this case, increasing temperatures and decreasing bulk lava SiO_2 contents directly reflect increasing proportions of the basaltic andesitic magma. At the same time, however, disaggregation of largely crystallized magma should have little effect on groundmass liquid or plagioclase rim compositions, especially if eruption rapidly follows. Thus, crystal–liquid equilibrium will be maintained in lavas with 'mixed' bulk compositions (e.g. Fig. 12).

DISCUSSION: SEQUENCE OF MAGMA CHAMBER EVOLUTION

Creation of shallow silicic chambers

The preponderance of large euhedral plagioclase phenocrysts and the presence of vesiculated basaltic andesitic magmatic inclusions in the Guadal andesitic and dacitic lavas are evidence that these silicic magmas resided in high-level chambers repeatedly fluxed by ascending mafic magmas. Evidence concerning the initial stages of silicic magma chamber

development is sparse, however. The presence of An-rich Type 2 plagioclase glomerocrysts suggests that the dacitic magmas were derived in part by remelting of plutonic rocks that initially crystallized from mafic, probably H_2O-rich magmas at high pressure. Conceivably, remelting and silicic magma production could have occurred at any crustal level. For example, the glomerocrysts containing An-rich plagioclase could have been plucked from deep crustal magma chambers and transported in rapidly ascending basaltic magmas similar to those erupted throughout the Tatara–San Pedro complex, as nearly all mafic lavas analyzed to date contain at least a few plagioclase phenocrysts with An-rich cores identical to those described here (M. A. Dungan & T. C. Feeley, unpublished data, 1996). Isolation of these grains in shallow crustal intrusions, followed by reheating and melting by successive inputs of basalt to the high-level system, could yield refractory cumulate fragments in direct contact with silicic partial melts (e.g. Heliker, 1995). Convective upward transport of the partial melts coupled with suspension of low-density plutonic fragments lacking mafic silicate phases might explain both the development of high-level silicic magma chambers and the absence of olivine in the glomerocrysts containing Type 2 plagioclase phenocrysts.

Alternatively, fractionation of basaltic magmas plus remelting of mafic intrusive rocks in the deep crust could produce silicic melts containing refractory An-rich plagioclase cumulate fragments (e.g. Hildreth & Moorbath, 1988). Separation from the deep crustal reservoirs, ascent, and stagnation of such evolved melts might also account for the development of high-level silicic reservoirs. This scenario is attractive because it invokes a common source region for the An-rich plagioclase crystals and the silicic magmas, and thus provides a convenient explanation for the flat core zoning profiles and the sharp contact between the An-rich and andesine zones (e.g. Fig. 10b, f). It does, however, require a complex scenario in which the deep crustal contribution to upper-crustal magma chambers alternates between silicic magmas and the more abundant mafic magmas that occur throughout the Tatara–San Pedro complex (Ferguson *et al.*, 1992). The questions of whether the dacitic magmas in the Guadal system were produced mainly in the deep or shallow crust, and to what extent they are fractionation products or partial melts are obviously important and will be addressed in a subsequent paper. At present, the mineralogic evidence and preceding lines of reasoning point to establishment of silicic magma chambers beneath the Guadal magmatic system in part through remelting of plutonic rocks that initially crystallized from hydrous mafic magmas in deep crustal differentiation zones.

Development of stratification within the shallow chambers

Figure 14 illustrates a suggested scheme for the origin of Guadal eruptive products following establishment of a high-level silicic magma chamber. The lack of strong zoning in Type 1 plagioclase phenocrysts and maintenance of textural and chemical equilibrium between Type 1 and 2 phenocryst rims and surrounding groundmass liquid indicate that the silicic liquids were not compositionally modified by mixing with mafic magmas. Furthermore, although the Nomarski images reveal the presence of a single or a few resorption surfaces in all Type 1 phenocryst cores, these surfaces are not associated with major compositional discontinuities or the development of sieve-textured regions (e.g. Fig. 10). They therefore more probably record dissolution of the plagioclase during events that gently heated the magmas, but which were not associated with compositional modification (Stamatelopoulou-Seymour *et al.*, 1990). We suggest that this stage is associated with injection and ponding of hot mafic magma at the base of the silicic magma chambers (Fig. 14), as has been proposed for many other calc-alkaline magma chambers (e.g. Eichelberger, 1975; Sparks *et al.*, 1977; Bacon & Druitt, 1988; Campbell & Turner, 1989; Pallister *et al.*, 1992; Feeley & Davidson, 1994; Tomiya & Takahashi, 1995). Apparently, in the Guadal magmatic system the volumes of individual mafic magma batches invading the upper-crustal chambers were insufficient relative to the volume of residing silicic magma to cause complete, chamber-wide hybridization (see Sparks & Marshall, 1986).

This is not to say, however, that mixing between recharged mafic magma and residing silicic magma did not occur. The textures and compositions of plagioclase phenocrysts in the magmatic inclusions have been shown to reflect incorporation of andesine-bearing silicic magma into basaltic magma, partial reaction of the phenocrysts, and subsequent precipitation of intermediate composition rims. Major and trace element trends defined by most of the magmatic inclusions also project along linear arrays defined by the andesitic magmas. The magmatic inclusion-forming magmas are thus best explained as hybrids formed by mixing partially crystallized dacitic magma with olivine-bearing, but plagioclase-poor basaltic magma. Conceivably, mixing and formation of the hybrid basaltic andesitic magma occurred because highly turbulent convection within

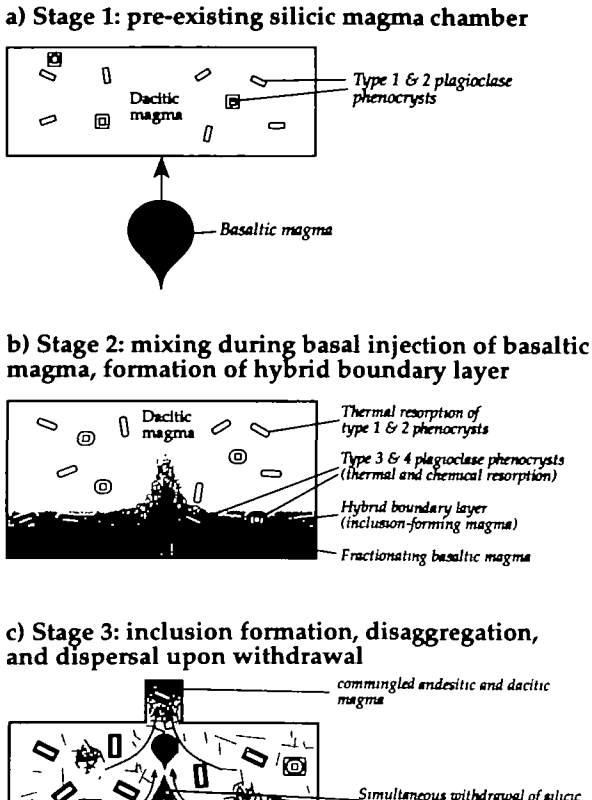

Fig. 14. Schematic model for producing the range of whole-rock, groundmass, and mineral compositions in Guadal volcanic rocks. (a) Stage 1: a high-level crustal magma chamber containing chemically homogeneous dacitic magma cools and precipitates Type 1 plagioclase phenocrysts and andesine rims around Type 2 An-rich phenocryst cores. (b) Stage 2: high-temperature, olivine-bearing (but plagioclase-poor) basaltic magma is injected into the base of the dacitic magma chamber. Highly turbulent convection along the mafic–silicic magma interface causes entrainment of plagioclase-saturated dacitic magma into basaltic magma and mixing at high mafic/silicic ratios. This forms a hybrid basaltic andesitic boundary layer. The bulk of the dacitic magma is chemically unaffected by this local mixing event, although Type 1 plagioclase phenocrysts are thermally resorbed. In hybrid basaltic andesitic magma, Type 3 and 4 plagioclase phenocrysts are created when andesine crystals derived from the dacitic magma partially dissolve and later precipitate a Ca-rich mantle during Stage 3. Basaltic recharge magma unaffected by mixing undergoes crystal fractionation at the base of the magma chamber. (c) Stage 3: withdrawal from the stratified chamber entrains small blobs of hybrid boundary layer magma into dacitic magma (e.g. Blake & Ivey, 1986). Undercooling of the basaltic andesitic magma followed by shearing and disaggregation of viscoelastic inclusions during or shortly before eruption disperses all components of magmatic inclusions into dacitic magma.

the injection fountain and along the mafic–silicic magma interface caused entrainment by viscous drag of dacitic magma into low-viscosity mafic magma (Fig. 14b; Campbell & Turner, 1989; Oldenburg *et al.*, 1989). In such a scenario the physical difficulty of mixing compositionally disparate magmas is surmounted because of locally high mafic to silicic magma ratios and the turbulent conditions along the interface.

Relative to most of the basaltic andesitic inclusions, the mafic lavas are depleted in MgO, Ni, and Cr (Fig. 2). We interpret these depletions to indicate that the mafic lavas represent crystal–liquid fractionation products little affected by the mixing process described above. Furthermore, because of their high modal plagioclase abundances and elevated Al_2O_3, Na_2O, and CaO contents, we infer that the mafic lavas accumulated plagioclase. Intriguingly, the few inclusions that show geochemical evidence for fractionation are not enriched in Al_2O_3, Na_2O, or plagioclase. Although speculative, this may reflect selective retention of plagioclase in the mafic lava-forming magmas because they were significantly more dense than the inclusion-forming magmas. Glazner & Ussler (1989) calculated that differentiation by olivine fractionation is less efficient than magma mixing in reducing liquid density. Therefore, fractionation of the basaltic magmas may have retarded lowering of their densities and inhibited separation of plagioclase.

A main conclusion assembled from all the above interpretations is that before eruption, the shallow Guadal magma chambers consisted of at least two and perhaps three compositionally and density stratified layers: a silicic upper layer, an intermediate layer consisting of hybrid basaltic andesitic magma, and possibly a lower layer consisting of fractionated basaltic magma (Fig. 14b). The relative volumes of the layers are unknown, but we surmise that a dominant volume (see Bacon & Druitt, 1988) of silicic magma may have been present, to inhibit chamber wide hybridization and to compositionally and thermally buffer the silicic magma during recharge events, thus producing the flat zoning profiles of the Type 1 plagioclase phenocrysts. Furthermore, as the Type 1 andesine phenocrysts in all of the andesitic and dacitic lavas are compositionally similar, the silicic upper layer at any time may have been fairly homogeneous. The X_{Ca}^{liq} of the silicic magma inferred from the core compositions of the Type 1 phenocrysts ranges from 0·18 to 0·25, assuming a value of three for K_D^{Ca-Na} (e.g. Fig. 12a). These values are slightly higher than the groundmass compositions of the andesitic and dacitic lavas (0·12–0·17; Table 2), which is consistent with crystallization of the plagioclase from dacitic or rhyolitic liquids slightly less evolved than liquids now represented by the groundmass glass.

The existence of a basal layer of fractionated mafic magma, although suggested by the presence of the

basaltic lavas and the evidence for recharge, is speculative because vent areas for the Guadal volcanic rocks are now buried by younger lavas erupted from Volcán Pellado. Thus, there is no direct evidence to support eruption of fractionated basaltic magma from the same chambers as those that produced the silicic lavas and hybrid inclusions. At the very least it seems unlikely that hot, dense mafic magmas could ascend unmodified through an upper-level chamber containing cool, low-density silicic magma. We therefore favor differentiation of these basaltic lavas in smaller, dominantly mafic chambers located on the periphery of the silicic system. The evidence for recharge and the physical barriers inhibiting thorough mixing of compositionally distinct magmas (except along the margins of the injection fountain; Campbell & Turner, 1989) nonetheless suggest that a significant fraction of newly injected basaltic magma may have ponded in a layer beneath the silicic layer, with a layer of hybrid magma between the two (Fig. 14b). The degree and style of fractionation of the basaltic magma in this environment, however, may not be the same as for the erupted basaltic lavas.

Withdrawal, inclusion formation, and the origin of compositional diversity

One of the most intriguing aspects of the Guadal andesitic and dacitic lavas is that many contain a large proportion of Type 2 plagioclase microphenocrysts that are too Ca rich to have precipitated in equilibrium from surrounding groundmass liquid. These crystals are compositionally and morphologically identical to the quench microphenocrysts and rims of plagioclase phenocrysts in coexisting magmatic inclusions. The most plausible and perhaps only explanation for these relationships is chilling of the basaltic andesitic hybrid magma followed by shearing and disaggregation of magmatic inclusions in dacitic magma (e.g. Thompson & Dungan, 1985; Koyaguchi, 1986; Clynne, 1996). As a result, all components of the inclusions were dispersed into dacitic magma in a surprisingly uniform manner. These include: (1) quench microphenocrysts of Ca-rich plagioclase and high-Mg, -Ti, and -Al pyroxene; (2) Type 3 and 4 plagioclase crystals with dusty sieve-textured zones and Ca-rich mantles; and (3) Mg-rich olivine phenocrysts. Evidence has also been presented that suggests mafic magma recharge, magma mixing, inclusion formation, and disaggregation were unique events that occurred in fairly rapid succession directly before or during eruption. For example, geochemical evidence for hybridization (and possibly fractionation) of inclusions, followed by dissolution and formation of sieve-textured zones on Type 3 and 4 plagioclase phenocrysts demonstrates that inclusion-forming magmas did not immediately chill upon injection into the silicic chambers. Conversely, the partial preservation of andesine cores in most of these phenocrysts also indicates that formation of the hybrid basaltic andesitic magma by liquid–liquid mixing took place shortly before undercooling and formation of the inclusions, according to estimates for rates of sodic plagioclase dissolution in calcic melt (Tsuchiyama, 1985). Furthermore, the transition from dissolution of the Type 3 and 4 phenocrysts to precipitation of Ca-rich euhedral mantles and similar composition acicular Type 2 groundmass microlites must reflect an abrupt shift from relatively moderate to rapid cooling of the hybrid magma (Lofgren & Norris, 1981). Finally, the lack of evidence for re-equilibration or resorption of xenocrysts derived from the magmatic inclusions suggests that disaggregation occurred at the onset of or during eruption.

A dynamic model that may account for the preceding observations is viscous coupling and entrainment of underlying hybrid basaltic andesitic magma into dacitic magma upon withdrawal from the stratified chamber (Fig. 14c; Blake & Ivey, 1986). Under these conditions, the entrained lower-viscosity hybrid mafic magma will disrupt into blobs of variable sizes and rapidly undercool to form largely solid inclusions (Rumscheidt & Mason, 1961; Sparks & Marshall, 1986; Tomiya & Takahashi, 1995). The degree and manner in which the magmatic inclusions may subsequently be disaggregated and dispersed through shear imposed by the host magma will be functions of the temperature and relative volume of mafic magma chilled, and hence the amount of heat released into the silicic magma body (Bacon & Metz, 1984; Thompson & Dungan, 1985; Koyaguchi, 1986). If the amount of mafic magma entrained is small, disaggregation will be limited because the silicic magma is heated little and the inclusion temperatures will rapidly fall near or possibly below the solidus. In this case, disaggregation may simply take the form of abrasion of chilled inclusion margins by crystals in the host magma. If the proportion of entrained mafic magma is large, however, inclusions may retain a significant fraction of interstitial melt because the equilibrium temperature may remain considerably above the solidus. In this case, wetting of grain boundaries by residual interstitial liquid will permit rapid and possibly complete disaggregation, leading to significant compositional and petrographic modification of the original host magma (Thompson & Dungan, 1985; Koyaguchi, 1986). The final equilibrium tem-

perature is dependent on the mass ratio and the thermodynamic values for the temperatures, heat capacities, and latent heats of the two magmas. We emphasize, however, that inferring a unique style of inclusion deformation and disaggregation from simple mass balance relationships may result in oversimplifications because mafic magma entrainment and heating of the silicic magma are gradual rather than instantaneous processes. Thus, whereas a lava may show bulk compositional evidence for addition of a large mafic component, it is possible that only during the latter stages of mafic magma entrainment will inclusions completely disaggregate because they retain significant quantities of residual interstitial liquid.

Petrographic–compositional relationships of the lavas are broadly consistent with the disaggregation model. For example, dacitic lavas have hypocrystalline textures, low calculated temperatures, high relative proportions of Type 1 andesine microphenocrysts, and whole-rock compositional trends that are separated from the andesitic lavas by a small gap in SiO_2 content. Conversely, they also contain high-Mg olivine xenocrysts and groundmass phases derived from the inclusions. These relations suggest that although the dacitic lavas have been modified to a small extent by inclusion disaggregation, a lower limit exists on the amount of mafic magma that must be entrained into silicic magma before large-scale inclusion disaggregation begins to be an important petrologic factor. In contrast, in lower-silica andesitic lavas only a very small percentage of the phenocrysts and microphenocrysts may represent crystals grown in the original dacitic magma. Except for small proportions of Type 1 andesine phenocrysts and microphenocrysts, the plagioclase frequency histograms for sample Gua13 are nearly identical to those for basaltic lava sample Gua14, which lies stratigraphically beneath it (Fig. 11). These similarities probably reflect extreme dilution of phenocryst phases grown in dacitic melt by addition of large amounts of largely crystallized basaltic magma. In this case, we infer that the basaltic andesitic magma was largely crystallized because this sample contains inclusions (e.g. Fig. 4b) and the Type 1 plagioclase phenocryst rims and groundmass grains have maintained equilibrium with surrounding groundmass liquid (Fig. 12b). The latter suggests that even in cases where large amounts of mafic magma are entrained into silicic magma bodies, the integrated style of inclusion disaggregation may involve insignificant amounts of residual liquid relative to the total mass of silicic liquid. This is consistent with the nearly holocrystalline nature of many inclusions. Alternatively, inclusion disaggregation could have involved a significant fraction of residual liquid, provided it was very similar in composition to the original dacitic melt. In either case, petrographic features of most Guadal andesitic lavas indicate that their phenocryst phases crystallized largely in dacitic magma, whereas their groundmass phases crystallized largely in hybrid basaltic andesitic magma. Thus, we suggest that mechanical blending of undercooled mafic magma and partially crystallized silicic magma should be considered as a possible mechanism for producing the common porphyritic texture of many calc-alkaline volcanic rocks, especially for those containing magmatic inclusions (Fig. 4).

SUMMARY AND IMPLICATIONS

Textural relationships and detailed mineral composition data for lavas and coexisting basaltic andesitic magmatic inclusions at Cordón El Guadal provide information on how magmas of differing temperatures and physical properties interact in shallow reservoirs beneath arc volcanoes. Basaltic lavas inferred to have erupted from vents located on the periphery of the Guadal silicic system have compositional and textural features suggesting a limited differentiation history dominated by fractionation of ferromagnesian silicate and oxide phases and retention of plagioclase. In contrast, data for silicic lavas and mafic magmas injected into the focus of the system record evidence for a complex history involving both liquid–liquid and solid–liquid mixing processes, and possibly fractionation of mineral phases. Specifically, compositions and textures of plagioclase phenocrysts in andesitic and dacitic lavas and coexisting basaltic andesitic inclusions indicate that inclusion-forming magmas are hybrids formed by mixing basaltic and dacitic or more silicic melts, whereas compositions of groundmass phases indicate that the andesitic and dacitic lavas are largely mechanical mixtures of dacitic magma and crystallized basaltic andesitic magma.

As at other locations, the style of mafic–silicic magma interaction at Cordón El Guadal was strongly dependent upon the relative proportions of the basaltic andesitic and silicic endmembers (Bacon & Metz, 1984; Koyaguchi, 1986; Sparks & Marshall, 1986). Guadal magmatic inclusions and silicic lavas form linear trends on SiO_2 variation diagrams, from which it can be inferred that the hybrid basaltic andesitic inclusions contain a larger component of the mafic endmember relative to the mechanically mixed andesitic lavas. Equally

important in the Guadal system, however, was the manner in which the contrasting magmas were juxtaposed. Textural evidence preserved in the plagioclase phenocrysts indicates that the transition from liquid–liquid to solid–liquid mixing was not continuous, but was partitioned into periods of magma chamber recharge and eruption, respectively. Evidently, during periods of recharge, basaltic magmas rapidly entrained small amounts of dacitic magma along the margins of turbulent injection fountains (Campbell & Turner, 1989). Conversely, during periods of eruption, dacitic magma gradually entrained small parcels of underlying hybrid basaltic andesitic magma. Thus, the coupled physical–chemical transition from mixed inclusions to commingled lavas is presumably not coincidental. It probably provides a partial record of the dynamic processes occurring in shallow magma chambers beneath continental arc volcanoes.

ACKNOWLEDGEMENTS

Work for this paper was supported by US NSF Grants EAR-9019441 and EAR-9206771, and Swiss Fonds National Grants 21-36509.92 and 2000-042124.94 to M.A.D. We thank François Bussy for initial help with the microprobe, Andrew Wulff and Mike Rhodes for supplying the XRF analyses, Jorge Lobato for help in the field, Anne Loi for assistance with manuscript preparation, and James Brophy and Michael Clynne for constructive, punctual reviews.

REFERENCES

Anderson, A. T., 1976. Magma mixing: petrological process and volcanological tool. *Journal of Volcanology and Geothermal Research* **1**, 3–33.

Anderson, A. T., 1983. Oscillatory zoning of plagioclase: Nomarski interference microscopy of etched polished sections. *American Mineralogist* **68**, 125–129.

Arculus, R. J. & Wills, K. J. A., 1980. The petrology of plutonic blocks and inclusions from the Lesser Antilles island arc. *Journal of Petrology* **21**, 43–99.

Bacon, C. R., 1986. Magmatic inclusions in silicic and intermediate volcanic rocks. *Journal of Geophysical Research* **91**, 6091–6112.

Bacon, C. R. & Druitt, T. H., 1988. Compositional evolution of the zoned calcalkaline magma chamber of Mount Mazama, Crater Lake, Oregon. *Contributions to Mineralogy and Petrology* **98**, 224–256.

Bacon, C. R. & Hirschmann, M. M., 1988. Mg/Mn partitioning as a test for equilibrium between coexisting Fe–Ti oxides. *American Mineralogist* **73**, 57–61.

Bacon, C. R. & Metz, J., 1984. Magmatic inclusions in rhyolites, contaminated basalts, and compositional zonation beneath the Coso volcanic field, California. *Contributions to Mineralogy and Petrology* **85**, 346–365.

Baker, D. R. & Eggler, D. H., 1983. Fractionation paths of Atka (Aleutians) high-alumina basalts: constraints from phase relations. *Journal of Volcanology and Geothermal Research* **18**, 387–404.

Baker, D. R. & Eggler, D. H., 1987. Compositions of anhydrous and hydrous melts coexisting with plagioclase, augite, and olivine or low-Ca pyroxene from 1 atm to 8 kbar: application to the Aleutian volcanic center of Atka. *American Mineralogist* **72**, 12–28.

Barnes, C. G., Johnson, K., Barnes, M. A., Prestvik, T., Kistler, R. V. & Sundvoll, B., 1995. The Greyback pluton: magmatism in a Jurassic back-arc environment, Klamath Mountains, Oregon. *Journal of Petrology* **36**, 397–416.

Beard, J. S., 1986. Characteristic mineralogy of arc-related cumulate gabbros: implications for the tectonic setting of gabbroic plutons and for andesite genesis. *Geology* **14**, 848–851.

Beard, J. S. & Borgia, A., 1989. Temporal variation of mineralogy and petrology in cognate gabbroic enclaves at Arenal volcano, Costa Rica. *Contributions to Mineralogy and Petrology* **103**, 110–122.

Blake, S. & Ivey, G. N., 1986. Magma-mixing and the dynamics of withdrawal from stratified reservoirs. *Journal of Volcanology and Geothermal Research* **27**, 153–178.

Blake, S., Wilson, C. J. N., Smith, I. E. M. & Walker, G. P. L., 1992. Petrology and dynamics of the Waimihia mixed eruption, Taupo volcano, New Zealand. *Journal of the Geological Society of London* **149**, 193–207.

Brophy, J. G., 1986. The Cold Bay volcanic center, Aleutian volcanic arc. *Contributions to Mineralogy and Petrology* **93**, 368–380.

Brophy, J. G., 1990. Andesites from northern Kanaga Island, Aleutians, implications of calc-alkaline fractionation mechanisms and magma chamber development. *Contributions to Mineralogy and Petrology* **104**, 568–581.

Campbell, I. H. & Turner, J. S., 1989. Fountains in magma chambers. *Journal of Petrology* **30**, 885–923.

Cioni, R., Civetta, L., Marianelli, P., Metrich, N., Santacroce, R. & Sbrana, A., 1995. Compositional layering and syn-eruptive mixing of a periodically refilled shallow magma chamber: the AD 79 plinian eruption of Vesuvius. *Journal of Petrology* **36**, 739–776.

Clynne, M. A., 1996. Complex magma mixing origin for multiple volcanic lithologies erupted in 1915, from Lassen Peak, California. *Journal of Petrology* (in press).

Corrigan, C. M., 1982. The crystal morphology of plagioclase feldspar produced during isothermal supercooling and constant rate cooling experiments. *Mineralogical Magazine* **46**, 433–439.

Crawford, A. J., Falloon, T. J. & Eggins, S., 1987. The origin of island arc high-alumina basalts. *Contributions to Mineralogy and Petrology* **97**, 417–430.

Davidson, J. P., Ferguson, K. M., Colucci, M. T. & Dungan, M. A., 1988. The origin and evolution of magmas from the San Pedro–Pellado Volcanic Complex, S. Chile: multicomponent sources and open system evolution. *Contributions to Mineralogy and Petrology* **100**, 429–445.

DeBari, S. M. & Coleman, R. G., 1989. Examination of the deep levels of an island arc: evidence from the Tonsina ultramafic–mafic assemblage, Tonsina, Alaska. *Journal of Geophysical Research* **94**, 4373–4391.

de Silva, S. L., 1989. The origin and significance of crystal rich inclusions in pumices from two Chilean ignimbrites. *Geological Magazine* **126**, 159–175.

Dungan, M. A. & Brown, R. W., 1977. The petrology of the Apollo 12 ilmenite basalt suite. *Proceedings of the 8th Lunar Science Conference*, pp. 1339–1381.

Eichelberger, J. C., 1975. Origin of andesite and dacite: evidence of mixing at Glass Mountain in California and other circum-Pacific volcanoes. *Geological Society of America Bulletin* **86**, 1381–1391.

Feeley, T. C. & Davidson, J. P., 1994. Petrology of calc-alkaline lavas at Volcán Ollagüe and the origin of compositional diversity at central Andean stratovolcanoes. *Journal of Petrology* **35**, 1295–1340.

Ferguson, K. M., Dungan, M. A., Davidson, J. P. & Colucci, M. T., 1992. The Tatara–San Pedro Volcano, 36°S, Chile: a chemically variable, dominantly mafic magmatic system. *Journal of Petrology* **33**, 1–43.

Freundt, A. & Schmincke, H.-U., 1992. Mixing of rhyolite, trachyte, and basalt magma erupted from a vertically and laterally zoned reservoir, composite flow P1, Gran Canaria. *Contributions to Mineralogy and Petrology* **112**, 1–19.

Frost, T. P. & Mahood, G. A., 1987. Field, chemical, and physical constraints on mafic–felsic magma interaction in the Lamarck Granodiorite, Sierra Nevada, California. *Geological Society of America Bulletin* **99**, 272–291.

Gamble, R. P. & Taylor, L. A., 1980. Crystal/liquid partitioning augite: effects of cooling rate. *Earth and Planetary Science Letters* **47**, 21–33.

Gardner, J. E., Carey, S., Rutherford, M. J. & Sigurdsson, H., 1995. Petrologic diversity in Mount St Helens dacites during the last 4,000 years: implications for magma mixing. *Contributions to Mineralogy and Petrology* **119**, 224–238.

Gerlach, D. C. & Grove, T. L., 1982. Petrology of Medicine Lake Highland volcanics: characterization of endmembers of magma mixing. *Contributions to Mineralogy and Petrology* **80**, 147–159.

Gerlach, D. C., Frey, F. A., Moreno-Roa, H. & Lopez-Escobar, L., 1988. Recent volcanism in the Puyehue–Cordon Caulle region, southern Andes, Chile (40·5°S): petrogenesis of evolved lavas. *Journal of Petrology* **29**, 333–382.

Ghiorso, M. S. & Sack, R. O., 1991. Fe–Ti oxide geothermometry: thermodynamic formulation and the estimation of intensive variables in silicic magmas. *Contributions to Mineralogy and Petrology* **108**, 485–510.

Gill, J. B. 1981. *Orogenic Andesites and Plate Tectonics*. Berlin: Springer-Verlag, 392 pp.

Glazner, A. F. & Ussler III, W., 1989. Crustal extension, crustal density, and the evolution of Cenozoic magmatism in the Basin and Range of the western United States. *Journal of Geophysical Research* **94**, 7952–7960.

Graham, I. J. & Worthington, T. J., 1988. Petrogenesis of Tauhara dacite (Taupo Volcanic Zone, New Zealand)—evidence for magma mixing between high-alumina andesite and rhyolite. *Journal of Volcanology and Geothermal Research* **35**, 279–294.

Grove, T. L. & Bence, A. E., 1977. Experimental study of pyroxene–liquid interaction in quartz-normative 15997. *Proceedings of the 8th Lunar Science Conference*, pp. 1549–1580.

Grove, T. L., Gerlach, D. C. & Sando, T. W., 1982. Origin of calc-alkaline series lavas at Medicine Lake volcano by fractionation, assimilation and mixing. *Contributions to Mineralogy and Petrology* **80**, 160–182.

Grunder, A. L. & Mahood, G. A., 1988. Physical and chemical models of zoned silicic magmas: the Loma Seca Tuff and Calabozos caldera, southern Andes. *Journal of Petrology* **29**, 831–867.

Heliker, C., 1995. Inclusions in Mount St. Helens dacite erupted from 1980 through 1983. *Journal of Volcanology and Geothermal Research* **66**, 115–135.

Hildreth, W. & Drake, R. E., 1992. Volcán Quizapu, Chilean Andes. *Bulletin of Volcanology* **54**, 93–125.

Hildreth, W. & Moorbath, S., 1988. Crustal contributions to arc magmatism in the Andes of central Chile. *Contributions to Mineralogy and Petrology* **98**, 455–499.

Housh, T. B. & Luhr, J. F., 1991. Plagioclase–melt equilibria in hydrous systems. *American Mineralogist* **76**, 477–492.

Huebner, J. S. & Sato, M., 1970. The oxygen fugacity relationships of manganese oxide and nickel oxide buffers. *American Mineralogist* **55**, 934–952.

Kilinc, A., Carmichael, I. S. E., Rivers, M. L. & Sack, R. O., 1983. The ferric–ferrous ratio of natural silicate liquids equilibrated in air. *Contributions to Mineralogy and Petrology* **83**, 136–140.

Koyaguchi, T., 1986. Textural and compositional evidence for magma mixing and its mechanism, Abu volcano group, Southwestern Japan. *Contributions to Mineralogy and Petrology* **93**, 33–45.

Kretz, R., 1982. Transfer and exchange equilibrium of a portion of the pyroxene quadrilateral as deduced from natural and experimental data. *Geochimica et Cosmochimica Acta* **46**, 411–422.

Langmuir, C. H., Vocke, R. D., Jr., Hanson, G. H. & Hart, S. R., 1978. A general mixing equation with applications to Icelandic basalts. *Earth and Planetary Science Letters* **37**, 380–392.

Lindsley, D. H., 1983. Pyroxene geothermometry. *American Mineralogist* **68**, 477–493.

Linneman, S. R. & Myers, J. D., 1990. Magmatic inclusions in the Holocene rhyolites of Newberry volcano, central Oregon. *Journal of Geophysical Research* **95**, 17677–17691.

Lofgren, G. E., 1974. An experimental study of plagioclase crystal morphology: isothermal crystallization. *American Journal of Science* **274**, 243–273.

Lofgren, G. E. & Norris, P. N., 1981. Experimental duplication of plagioclase sieve and overgrowth textures. *Geological Society of America Abstracts with Programs* **13**, 498.

Luhr, J. F., 1992. Slab-derived fluids and partial melting in subduction zones: insights from two contrasting Mexican volcanoes (Colima and Ceboruco). *Journal of Volcanology and Geothermal Research* **54**, 1–18.

McMillan, M. J. & Dungan, M. A., 1986. Magma mixing as a petrogenetic process in the development of the Taos Plateau volcanic field, New Mexico. *Journal of Geophysical Research* **91**, 6029–6045.

Nakada, S., Bacon, C. R. & Gartner, A. E., 1994. Origin of phenocrysts and compositional diversity in pre-Mazama rhyodacite lavas, Crater Lake, Oregon. *Journal of Petrology* **35**, 127–162.

Nakamura, M., 1995. Continuous mixing of crystal mush and replenished magma in the ongoing Unzen eruption. *Geology* **23**, 807–810.

Oldenburg, C. M., Spera, F. J., Yuen, D. A. & Sewell, G., 1989. Dynamic mixing in magma bodies: theory, simulations, and implications. *Journal of Geophysical Research* **94**, 9215–9236.

Pallister, J. S., Hoblitt, R. P. & Reyes, A. G., 1992. A basalt trigger for the 1991 eruptions of Pinatubo volcano? *Nature* **356**, 426–428.

Panjasawatwong, Y., Danyushevsky, L. V., Crawford, A. J. & Harris, K. L., 1995. An experimental study of the effects of melt composition on plagioclase–melt equilibria at 5 and 10 kbar: implications for the origin of magmatic high-An plagioclase. *Contributions to Mineralogy* **118**, 420–432.

Peccerillo, A. & Taylor, S. R., 1976. Geochemistry of Eocene calc-alkaline volcanic rocks from the Kastamonu area, northern Turkey. *Contributions to Mineralogy and Petrology* **58**, 63–81.

Rhodes, J. M., 1988. Geochemistry of the 1984 Mauna Loa eruption: implications for magma storage and supply. *Journal of Geophysical Research* **93**, 4453–4466.

Roeder, R. L. & Emslie, R. F., 1970. Olivine–liquid equilibrium. *Contributions to Mineralogy and Petrology* **29**, 275–289.

Rumscheidt, F. D. & Mason, S. G., 1961. Particle motion in sheared suspensions XII. Deformation and burst of fluid drops in shear and hyperbolic flow. *Journal of Colloid Science* **16**, 238–261.

Schiffman, P. & Lofgren, G. E., 1982. Dynamic crystallization studies on the Grande Ronde pillow basalts, central Washington. *Journal of Geology* **90**, 49–78.

Singer, B. S., Thompson, R. A., Dungan, M. A., Feeley, T. C., Pickens, J. Brown, L. L., Nelson, S. T., Wulff, A. W., Davidson, J. P. & Metzger, J., 1996. *930 Thousand Years of Volcanism and Erosion at the Tatara–San Pedro Complex, Chilean Andes: a Geochronologic, Paleomagnetic, and Geochemical Record*. Boulder, CO: Geological Society of America, in press.

Sisson, T. W. & Grove, T. L., 1993. Experimental investigations of the role of H_2O in calc-alkaline differentiation and subduction zone magmatism. *Contributions to Mineralogy and Petrology* **113**, 143–166.

Sparks, R. S. J. & Marshall, L. A., 1986. Thermal and mechanical constraints on mixing between mafic and silicic magmas. *Journal of Volcanology and Geothermal Research* **29**, 99–124.

Sparks, R. S. J., Sigurdsson, H. & Wilson, L., 1977. Magma mixing: a mechanism for triggering acid explosive eruptions. *Nature* **267**, 315–318.

Stamatelopoulou-Seymour, K., Vlassopoulos, D., Pearce, T. H. & Rice, C., 1990. The record of magma chamber processes in plagioclase phenocrysts at Thera Volcano, Aegean Volcanic Arc, Greece. *Contributions to Mineralogy and Petrology* **104**, 73–84.

Thompson, R. A. & Dungan, M. A., 1985. The petrology and geochemistry of the Handkerchief Mesa mixed magma complex, San Juan Mountains, Colorado. *Journal of Volcanology and Geothermal Research* **26**, 251–274.

Tomiya, A. & Takahashi, E., 1995. Reconstruction of an evolving magma chamber beneath Usu Volcano since the 1663 eruption. *Journal of Petrology* **36**, 617–636.

Tormey, D. R., Frey, F. A. & Lopez-Escobar, L., 1995. Geochemistry of the active Azufre–Planchon–Peteroa volcanic complex, Chile (35°15′S): evidence for multiple sources and processes in a Cordilleran arc magmatic system. *Journal of Petrology* **36**, 265–298.

Tsuchiyama, A., 1985. Dissolution kinetics of plagioclase in the melt of the system diopside–albite–anorthite, and the origin of dusty plagioclase in andesites. *Contributions to Mineralogy and Petrology* **89**, 1–16.

Wallace, P. J. & Carmichael, I. S. E., 1994. Petrology of Volcán Tequila, Jalisco, Mexico: disequilibrium phenocryst assemblages and evolution of the subvolcanic magma system. *Contributions to Mineralogy and Petrology* **117**, 345–361.

Wells, P. R. A., 1977. Pyroxene thermometry in simple and complex systems. *Contributions to Mineralogy and Petrology* **62**, 129–139.

Wood, B. J. & Banno, S., 1973. Garnet–orthopyroxene and orthopyroxene–clinopyroxene relations in simple and complex systems. *Contributions to Mineralogy and Petrology* **42**, 109–124.

RECEIVED APRIL 11, 1996
REVISED TYPESCRIPT ACCEPTED JULY 15, 1996